*J. Fluid Mech.* (2004), *vol.* 518, *pp.* 95–123.  
DOI: 10.1017/S0022112004000989 Printed in the United Kingdom

# Response of the wake of an isolated particle to an isotropic turbulent flow

By PROSENJIT BAGCHI† AND S. BALACHANDAR

Department of Theoretical and Applied Mechanics, University of Illinois at Urbana-Champaign, Urbana, IL 61801, USA

(Received 7 January 2004 and in revised form 25 May 2004)

The interaction of an isolated spherical particle with an isotropic turbulent flow is considered using direct numerical simulations (DNS). The particle Reynolds number is varied from about 50 to 600 and the particle diameter is varied from about 1.5 to 10 times the Kolmogorov scale. The Reynolds number based on the Taylor microscale of the free-stream turbulent field considered here is 164. The DNS technique employed here is the first of its kind to address particle–turbulence interaction and it resolves the smallest scales in the free-stream turbulent flow and the complex vortical structures in the particle wake. The primary objective of this paper is to present new results on the effect of the free-stream turbulence on the particle wake and vortex shedding, and the modulation of free-stream turbulence in the particle wake. The parameters of the present simulations are comparable to those of the experimental study by Wu & Faeth (1994*a*, *b*), and agreement between the present computational results and the experimental measurement is demonstrated.

The effect of free-stream turbulence on the mean and instantaneous wake structure is studied. The time-averaged mean wake in a turbulent ambient flow shows a lower velocity deficit and a flatter profile. However, in agreement with the experimental results of Wu & Faeth the mean wake in a turbulent flow behaves like a self-preserving laminar wake. At Reynolds numbers below about 210 the effect of free-stream turbulence is to introduce wake oscillations. For Reynolds numbers in the range 210 to 280, free-stream turbulence is observed to promote early onset of vortex shedding. The nature of the shed vortices is somewhat different from that in a uniform flow. Increasing the free-stream turbulence intensity suppresses the process of vortex shedding, and only marginally increases the wake oscillation. The modulation of free-stream turbulence in the wake is studied in terms of the distribution of kinetic energy and RMS velocity fluctuation. The free-stream energy lost in the wake is recovered faster in a turbulent ambient flow than in a uniform ambient flow. The energy of the velocity fluctuation is enhanced in the wake at low free-stream intensities, and is damped or marginally increased at higher intensities. The fluctuation energy is not equi-partitioned among the streamwise and cross-stream components. The RMS streamwise fluctuation is always enhanced, whereas the RMS cross-stream fluctuation is enhanced only at low free-stream intensities, and damped at higher intensities.

## 1. Introduction

Turbulence modulation by particles is an important aspect of two-phase flow research. It has been well established that the addition of particles can increase or

† Present address: Department of Mechanical and Aerospace Engineering, Rutgers University, Piscataway, NJ 08854; pbagchi@jove.rutgers.edu

reduce the level of turbulence in the fluid phase. In a dilute suspension there are several mechanisms that contribute to turbulence modulation: (i) enhanced dissipation due to the presence of particles, (ii) transfer of kinetic energy to the fluid from the particles, (iii) formation of wakes and shedding of vortices behind the particles. The relative importance of these mechanisms depends on the parameters of the problem: particle-to-turbulence length-scale ratio, particle Reynolds number, particle-to-fluid density ratio, etc. When particles are smaller than the Kolmogorov scale, their Reynolds number is generally less than unity, and only the first two mechanisms are significant. In this range, particles draw energy from the large scales thereby causing dissipation at these scales. The motion of particles, in turn, returns energy to small scales causing energy enhancement at these scales. For larger particles, the third mechanism is also important since fluctuations created by wake oscillation and vortex shedding may add energy to the fluid turbulence.

In numerical studies of turbulence modulation, the particles are often modelled as point forces (Squires & Eaton 1991; Elghobashi & Truesdell 1993; Boivin, Simonin & Squires 1998). In the interest of simulating the effect of a very large number of particles the details of flow at the microscale around each particle is ignored. This approach becomes increasingly accurate for particles of size much smaller than the Kolmogorov scale. But there are many situations where the particle size is of the order of Kolmogorov scale or larger, and correspondingly the particle Reynolds number is larger than unity. The effect of finite particle size, particle wake, and vortex shedding are important in this range. Hetsroni (1989) suggested that in this range natural shedding of vortices from the particle, above a particle Reynolds number of about 400, is mostly responsible for turbulence augmentation. Experiments and recent numerical simulations show that vortex shedding starts at a somewhat lower Reynolds number of around 280 (Magarvey & Bishop 1961; Natarajan & Acrivos 1993; Johnson & Patel 1999; Tomboulides & Orszag 2000). It is however not known how the natural vortex shedding process is influenced by free-stream turbulence.

Mittal (2000) recently performed direct numerical simulations of a sinusoidally oscillating uniform flow over a single stationary particle. By systematically varying the amplitude and frequency of the free-stream oscillation, he showed that natural vortex shedding is not the only mechanism of turbulence enhancement. He observed that at Reynolds numbers below 300, oscillation in the free-stream generates a resonant oscillation in the wake, which enhances the kinetic energy in the wake. A flow visualization of the wake showed that at a Reynolds number as low as 150, $\Lambda$-shaped vortices are formed which have completely different topology from those observed in natural vortex shedding. Above a Reynolds number of about 300, turbulence enhancement in the wake is primarily by natural vortex shedding. But as the strength of free-stream oscillation increases, the resonance mechanism can be dominant. The spectrum of energy in a turbulent flow is, however, quite broad, and the three-dimensional structure of turbulent flow cannot be represented by simple sinusoidal oscillations.

By analysing a collection of experimental results, Gore & Crowe (1989) proposed that the ratio of particle diameter to characteristic size of the energy-containing eddies in the carrier phase is the key parameter that dictates turbulence modulation. They concluded that when this ratio is above 0.1, particles augment turbulence, and attenuate it otherwise. Numerical simulations of finite-sized particles in wall turbulence by Pan & Bannerjee (1997) generally support the above proposal. Table 1 lists the parametric range of some experimental works on particle–turbulence interaction. A variety of flows, such as a particle-laden jet, a pipe flow, a channel flow and a backward-facing step, have been studied. In many of these experiments the particle

| Author | Experiments | $d/\eta$ | $d/\lambda$ | $I$ | $\langle Re_r \rangle$ |
|---|---|---|---|---|---|
| TMS | Pipe flow | 2–60 | 0.13–2 | 0.05–0.15 | |
| WF | Homogeneous turbulence | 1.2–12 | 0.13–2 | 0.04–0.07 | 135–1560 |
| PF | Homogeneous turbulence | 1.2–8 | | 0.02–0.08 | 38–545 |
| TMTKN | Particle-laden jet | | | 0.05–0.15 | 100–750 |
| LE | Particle-laden jet | $7–29^+$ | | | |
| KFE | Channel flow | $0.57–3^+$ | | 0.05–0.2 | 5–20 |
| BGM | Stirred vessel | 1.5–35 | | | 0.2–40 |

TABLE 1. Some experimental works on particle–flow interaction and their parametric range. Here $^+$ indicates that the number is $\tau_p/\tau_f$, the ratio of particle response time to fluid time scale. TMS: Tsuji *et al.* (1984); WF: Wu & Faeth (1994*a*, *b*); PF: Parthasarathy & Faeth (1990); TMTKN: Tsuji *et al.* (1988); LE: Longmire & Eaton (1992); KFE: Kulick *et al.* (1994); BGM: Brucato *et al.* (1998). $d$ = particle diameter, $\eta$ = Kolmogorov scale; $\lambda$ = Taylor microscale. $\langle Re_r \rangle$ is particle Reynolds number based on the mean relative velocity, and $I$ is the intensity of the free-stream turbulent flow defined as the ratio of the RMS turbulent fluctuations and a steady oncoming uniform flow (defined in § 2).

size is bigger than the Kolmogorov scale, or of the order of the Taylor microscale. These studies support the general trend that large particles and increased mass loading augment turbulence.

Of particular relevance to the present study is the work of Wu & Faeth (1994*a*) where the effect of free-stream homogeneous turbulence on the particle wake and vortex shedding is considered. They observed that at a low free-stream turbulence intensity of about 4% the wake becomes turbulent even at low Reynolds numbers, and the streamwise RMS velocity fluctuations in the wake are substantially more enhanced than the cross-stream fluctuations. At higher Reynolds numbers, the natural vortex shedding was not disturbed by free-stream turbulence, and the RMS fluctuations in the streamwise and cross-stream directions were comparable. Wu & Faeth (1994*b*) considered the effect of increasing the intensity of free-stream turbulence. Their results suggest that at moderate-to-high particle Reynolds numbers with increasing turbulence intensity, the increase in cross-stream fluctuation is reduced.

In the present work we consider the interaction of a free-stream isotropic turbulent flow with a single isolated stationary spherical particle. The present numerical simulations, thus, complement the experiments of Wu & Faeth (1994*a*). Parameters, such as particle-to-turbulence length scale and particle Reynolds number, chosen for the present investigation are in the range of those employed by Wu & Faeth (1994*a*) in their experiment (see table 1). The range of the particle Reynolds number considered here is 58 to 610, and the ratio of the particle diameter to Kolmogorov scale $d/\eta$ is 1.53 to 9.59. The microscale Reynolds number of the free-stream turbulent flow is kept fixed at 164 for all the cases. The range of the particle Reynolds number considered in our study covers three different regimes of wake evolution in a uniform flow: steady axisymmetric wake, steady non-axisymmetric wake, and unsteady vortex shedding. In the non-axisymmetric and unsteady regime, the wake exhibits complex three-dimensional vortical structures. The wake structure can be expected to become further complicated in the presence of free-stream turbulence.

Any numerical method aimed at understanding particle–turbulence interaction must be able to fully resolve the wake structure. We employ a direct numerical simulation (DNS) technique that uses a high-resolution fully spectral methodology for this purpose. The DNS methodology resolves the complete details of the particle

wake, as well as all the scales of free-stream turbulence. The objective of this paper is to present results on the effect of free-stream isotropic turbulence on mean and instantaneous wake structure. Particular attention will be paid to understanding how free-stream turbulence influences vortex shedding, and consequently, how free-stream turbulence is modulated. The particle-to-particle and wake-to-wake interaction effects are not considered here. The DNS technique and the results presented here are the first of their kind on particle–turbulence interaction.

## 2. Simulation technique

We consider a stationary particle subjected to a frozen isotropic turbulent field $\boldsymbol{U}(\boldsymbol{X})$ superimposed on a uniform flow $\boldsymbol{V}$. The isotropic turbulent field is obtained from a separate computation by Langford (2000) using a $256^3$ grid in a cubic box. The field is periodic in all three directions and hence can be extended to any arbitrary large volume. The important length and velocity scales of the isotropic turbulence (non-dimensionalized in terms of Kolmogorov length and velocity scales, $\eta$ and $v_k$) are as follows: RMS of the turbulent velocity fluctuation ($U_{rms}/v_k$) is 6.5, the periodic box size ($L/\eta$) is 757, Taylor microscale $\lambda/\eta$ is 25.2. The single parameter that characterizes this isotropic turbulent field is the microscale Reynolds number $Re_\lambda = 164$.

An instantaneous realization $\boldsymbol{U}(\boldsymbol{X})$ of the isotropic field is taken, where $(X, Y, Z)$ represents a fixed reference frame. The turbulent field is superposed on a steady uniform free stream $\boldsymbol{V}$. In other words, the turbulent field $\boldsymbol{U}(\boldsymbol{X})$ is swept over the stationary particle at velocity $\boldsymbol{V}$. Thus in a reference frame attached to the particle, the frozen turbulent field appears as both space- and time-varying. Without loss of generality we assume that $\boldsymbol{V}$ is oriented along the $X$-axis. The computational domain attached to the particle is a spherical domain $(r, \theta, \phi)$ whose outer radius $R_O$ is 30 times the radius of the particle. The undisturbed ambient flow, as seen by the particle as $\boldsymbol{V} + \boldsymbol{U}(\boldsymbol{x} + \boldsymbol{X}_p(t))$, is specified at the inflow section of this outer boundary. Here $\boldsymbol{X}_p(t) = \boldsymbol{X}_p(0) - \boldsymbol{V}\,t$ is the instantaneous location of the centre of the particle in the frame of the isotropic field. A schematic view of the computation domain attached to the particle and the precomputed turbulent field is shown to scale in figure 1 for the case of $d/\eta = 10$. In general, the grid points of the spherical computational domain attached to the particle do not coincide with the grid points of the $(2\pi)^3$ cubic box in which the isotropic turbulent field is computed. Thus the turbulent velocity field $\boldsymbol{U}(\boldsymbol{X})$ has to be interpolated on to the outer boundary of the spherical domain. In order to retain spectral accuracy, the interpolation is done using the Fourier summation.

It must be stressed that here we use an instantaneous three-dimensional field of precomputed isotropic turbulence to supply the turbulent inflow condition for the particle. Instead, an inflow could have been constructed as a uniform flow with superposition of a spectrum of modes with time-varying amplitudes to mimic the desired turbulence properties. Although somewhat computationally complicated, the application of the precomputed frozen isotropic box turbulence as the inflow condition provides a well-defined turbulent ambient flow which is characterized by a single parameter, the microscale Reynolds number.

In the spherical domain attached to the particle, the governing (continuity and Navier–Stokes) equations are solved by a direct numerical simulation. A Fourier–Chebyshev collocation scheme in the spherical coordinates ($d/2 \leqslant r \leqslant R_0$, $0 \leqslant \theta \leqslant \pi$, $0 \leqslant \phi \leqslant 2\pi$) is used for the spatial discretization, and a two-step time-split scheme is used for the temporal discretization. Specifically, we use Chebyshev collocation in the radial direction, and Fourier collocation in the azimuthal direction.

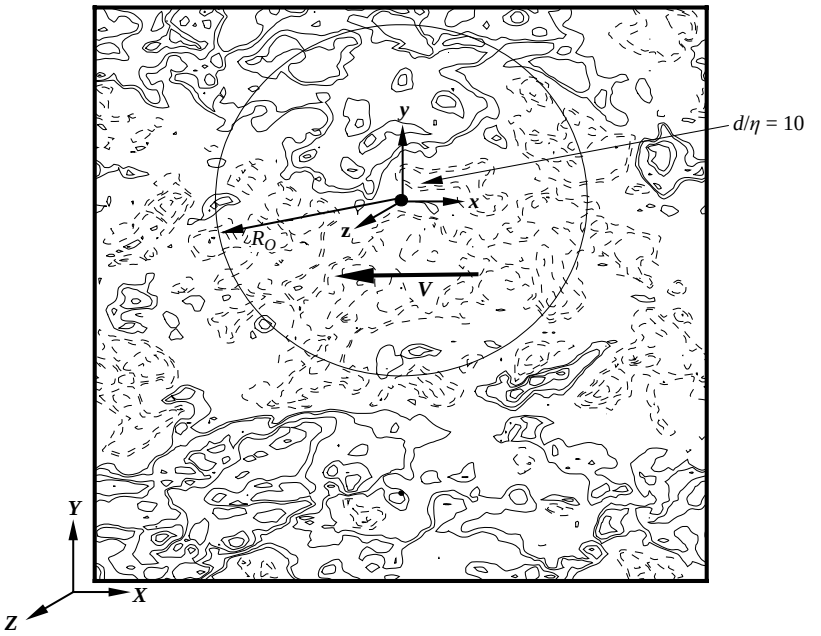


FIGURE 1. Schematic of the particle–flow configuration. Drawn to the true scale, a particle of $d/\eta = 10$ is shown here. The large circle surrounding the particle represents the outer boundary of the spherical computational domain attached to the particle. The outer box represents the periodic box in which the isotropic turbulent flow is generated. Contours of one cross-stream velocity component scaled by the mean relative velocity $\langle |\boldsymbol{V}_r| \rangle$ are shown for free-stream turbulent intensity $I = 0.1$.

In the tangential ($\theta$) direction, sine or cosine expansions are used. Further details about the collocation method are given in Bagchi (2002) and Bagchi & Balachandar (2002). At the outflow boundary of the spherical domain, a non-reflecting boundary condition described by Mittal & Balachandar (1996) is used. On the surface of the particle no-slip and no-penetration conditions are satisfied. The distribution of the grid points is non-uniform: they are clustered near the surface of the particle and in the wake region. The grid resolution is chosen to satisfy two criteria: first, the size of the largest grid spacing in the spherical domain is less than that of the grid used to simulate the isotropic turbulent field, in order to guarantee resolution of the free-stream turbulence; second, the grid is adequate to resolve the thin shear layers and the wake structures generated by the particle. Typical grids used in the simulation have 141 points in the radial direction, 160 in the $\theta$-direction and 128 in the $\phi$-direction.

In order to obtain well-converged statistics, the entire length $L$ of the cubic box of turbulence is passed over the particle several times. This ensures that any initial transience from the start-up decays, and that a long-time periodic behaviour is established. The length of the turbulence box can vary from about 150 to 1000 times the diameter of the particle. A typical dimensionless time-step $\Delta t|\boldsymbol{V}|/d$ used in the simulations is 0.0005. Thus the total number of time-steps for which time integration is performed is of the order of $10^6$. This combined with the high grid resolution renders the computations very expensive. A typical computational time for a simulation is about 20 000 CPU hours on Origin2000 supercomputers using 32 processors.

| Case | $d/\eta$ | $d/\lambda$ | $d/\Lambda$ | $\langle Re_r \rangle$ | $I$ | $\tilde{I}$ |
|---|---|---|---|---|---|---|
| Case 1 | 1.53 | 0.061 | 0.003 | 107 | 0.1 | 0.093 |
| Case 2 | 1.53 | 0.061 | 0.003 | 58 | 0.2 | 0.171 |
| Case 3 | 3.84 | 0.152 | 0.008 | 261 | 0.1 | 0.096 |
| Case 4 | 3.84 | 0.152 | 0.008 | 114 | 0.25 | 0.219 |
| Case 5 | 9.59 | 0.381 | 0.019 | 610 | 0.1 | 0.103 |
| Case 6 | 9.59 | 0.381 | 0.019 | 241 | 0.25 | 0.259 |

TABLE 2. Parametric range of the present study. $\Lambda$ is the integral scale and $\tilde{I}$ is the ratio of the RMS turbulent fluctuations and the mean relative velocity between the particle and the flow.

The time-averaged mean quantities are obtained by averaging over a time $T$ required to sweep the periodic box of turbulence past the stationary particle. The mean quantities are denoted by the symbol $\langle\rangle$. Accumulation of statistics is performed by storing the velocity field at regular time intervals. The two key input parameters of the simulation are the non-dimensional particle size, $d/\eta$, and the relative strength of free-stream turbulence, measured in terms of $I = U_{rms}/|\boldsymbol{V}|$. The other important parameter is the particle Reynolds number, $\langle Re_r \rangle = |\langle \boldsymbol{V}_r \rangle| d/\nu$, which can be expressed in terms of the above two input parameters as

$$\langle Re_r \rangle = \frac{d/\eta}{U_{rms}/\boldsymbol{V}} \frac{U_{rms}}{v_k} \frac{|\langle \boldsymbol{V}_r \rangle|}{\boldsymbol{V}}. \tag{2.1}$$

The Reynolds number is defined in terms of the mean relative velocity, where $\boldsymbol{V}_r = \boldsymbol{V} + \boldsymbol{U}(\boldsymbol{X}_p(t))$ is the instantaneous relative velocity between the particle and the undisturbed ambient flow measured at the centre of the particle and $|\langle \boldsymbol{V}_r \rangle|$ is the mean obtained by time-averaging over $T$. Note that although the isotropic turbulent velocity field averaged over the entire box is guaranteed to be zero, the mean turbulent velocity seen by the particle, $\langle \boldsymbol{U}(\boldsymbol{X}_p(t)) \rangle$, may be non-zero due to the limited volume sampled by the particle and as a result $|\langle \boldsymbol{V}_r \rangle| \neq \boldsymbol{V}$. The ratio $|\langle \boldsymbol{V}_r \rangle|/\boldsymbol{V}$ is thus generally around 1, and its precise value depends on the section of isotropic turbulence passed over the particle. The ratio $U_{rms}/v_k$ depends on the isotropic turbulence and in the present simulation its value is fixed at 6.5. Table 2 presents the values of $d/\eta$, $\langle Re_r \rangle$ and $I$ for the six different simulations considered in this study. In all the cases considered the particle is bigger than the Kolmogorov scale but smaller than the Taylor microscale. Also shown in the table is $\tilde{I} = U_{rms}/|\langle \boldsymbol{V}_r \rangle|$. For each of the six cases shown in table 2 a companion simulation was also performed at the same mean Reynolds number, $\langle Re_r \rangle$, but in a uniform flow. Thus results from a total of 12 simulations will be discussed below.

The accuracy of the numerical scheme used here has been tested in a number of situations, from uniform turbulence-free flows to shear flows to turbulent flows. These results are reported in Bagchi (2002) and Bagchi & Balachandar (2002) for non-turbulent cases, and in particular in Bagchi & Balachandar (2003) for the six turbulent flow simulations to be reported here. Specifically, in Bagchi & Balachandar (2003), we discuss the grid-independence, the decay of energy spectra, the effect of the size of the computation boundary, and the effect of changing the time-averaging window $T$. Hence, they will not be repeated in this paper. Additional comparisons of our DNS results with the experiments of Wu & Faeth (1994*a*, *b*) are given in the next section (figures 4 and 21) which show good agreement between the two.

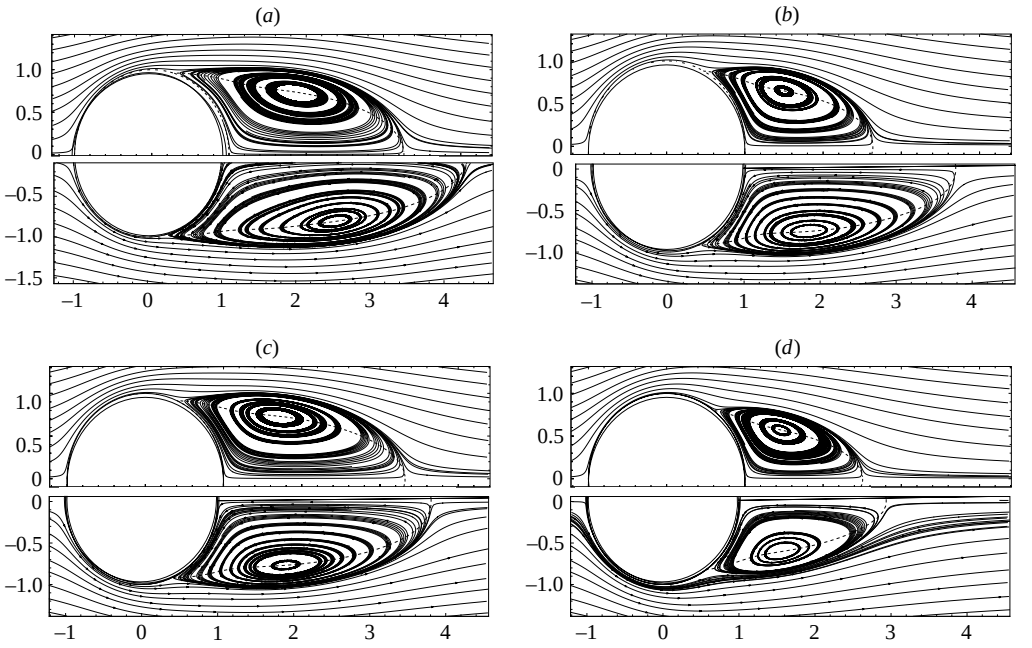


FIGURE 2. Mean wake structure. For each figure, the top half is the turbulent inflow case, and the bottom half is the uniform inflow case. (*a*) Case 5 ($d/\eta = 9.59$, $\langle Re_r \rangle = 610$); (*b*) case 6 ($d/\eta = 9.59$, $\langle Re_r \rangle = 241$); (*c*) case 3 ($d/\eta = 3.84$, $\langle Re_r \rangle = 261$); (*d*) case 1 ($d/\eta = 1.53$, $\langle Re_r \rangle = 107$).

## 3. Results and discussion

### 3.1. *Mean wake*

Mean streamlines are shown in figure 2 for cases 1, 3, 5 and 6. They are obtained by averaging the instantaneous velocity field in time and in the azimuthal direction $\phi$ ($0 \leqslant \phi \leqslant 2\pi$). The wake structure in free-stream turbulence is compared with that in zero-turbulence uniform flow at the same Reynolds number. The results show that the mean recirculation region is shorter in a turbulent flow than in a uniform flow. Quantitative results on wake length are shown in figure 3. The general trend is that the wake length is shortened as the level of turbulence increases, and the effect is more substantial at high $\langle Re_r \rangle$ than at low $\langle Re_r \rangle$.

The mean streamwise velocity along the $x$-axis is shown in figure 4 for case 1 ($d/\eta = 1.53$, $I = 0.1$, $\langle Re_r \rangle = 107$) and case 5 ($d/\eta = 9.59$, $I = 0.1$, $\langle Re_r \rangle = 610$). The results for non-turbulent free stream at the corresponding Reynolds numbers are also shown. For both cases, the streamwise velocity along the axis is higher in the turbulent flow than in the non-turbulent flow, due to enhanced mixing in the wake in the presence of free-stream turbulence. The effect is more pronounced at lower $\langle Re_r \rangle$ than at higher $\langle Re_r \rangle$, since in the latter case the wake is chaotic even in a uniform flow. Also shown in figure 4 is the comparison of the DNS results with the experimental results obtained by Wu & Faeth (1994*a*). While the agreement is good, a perfect match is not obtained. We note that the intensity of the free-stream turbulence considered in the experiment is less than in our DNS study. Thus, it is not surprising that the wake velocity recovers at a slower rate in their case than in the DNS.

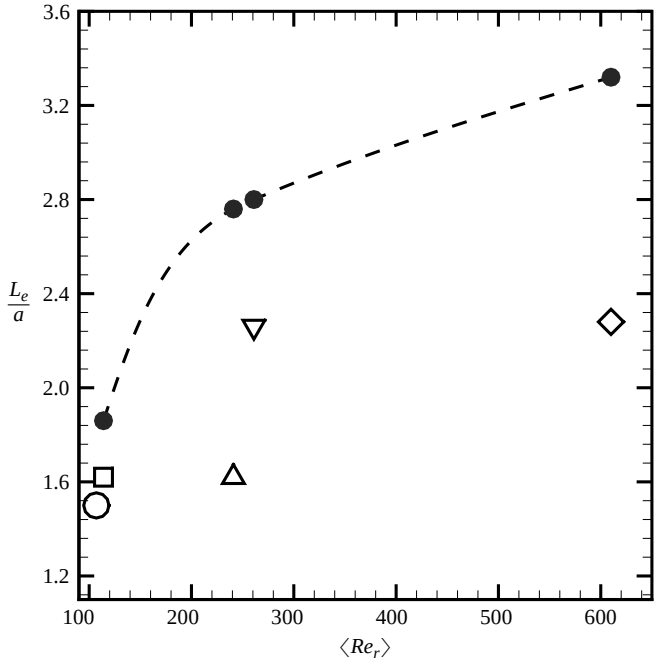


FIGURE 3. Effect of turbulence on the length $L_e$ of the recirculation region. Solid circles are the uniform-flow results. □, Case 1 ($d/\eta = 1.53$, $I = 0.1$, $\langle Re_r \rangle = 107$); ▽, case 3 ($d/\eta = 3.84$, $I = 0.1$, $\langle Re_r \rangle = 261$); ○, case 4 ($d/\eta = 3.84$, $I = 0.25$, $\langle Re_r \rangle = 114$); ◇, case 5 ($d/\eta = 9.59$, $I = 0.1$, $\langle Re_r \rangle = 610$); △, case 6 ($d/\eta = 9.59$, $I = 0.25$, $\langle Re_r \rangle = 241$).

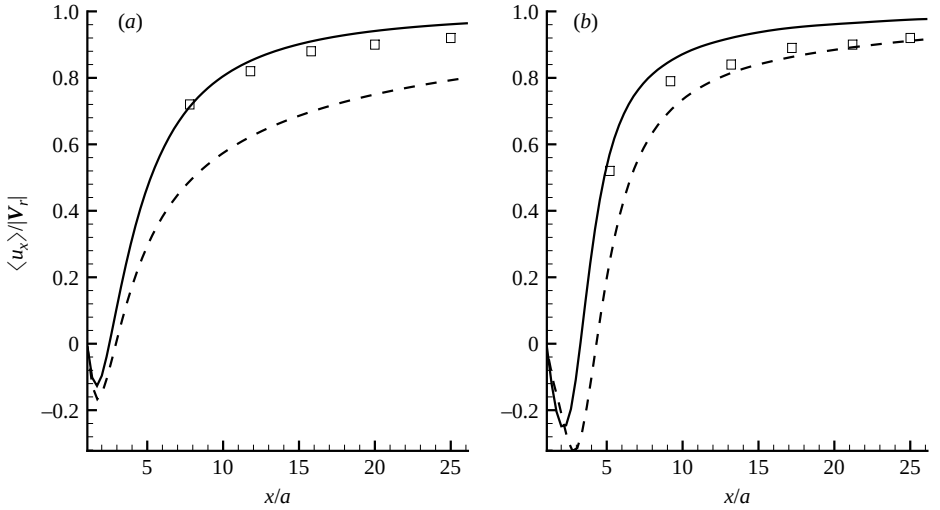


FIGURE 4. Mean streamwise velocity along the $x$-axis. DNS results: ($a$) case 1 ($d/\eta = 1.53$, $I = 0.1$, $\langle Re_r \rangle = 107$); ($b$) case 5 ($d/\eta = 9.59$, $I = 0.1$, $\langle Re_r \rangle = 610$). ——, Turbulent flow; - - - - -, uniform flow. □, Experimental results (Wu & Faeth (1994*a*). The experimental data for case 1 were obtained at $\langle Re_r \rangle = 135$, $d/\eta = 1.25$, $\tilde{I} = 0.04$, and for case 5 at $\langle Re_r \rangle = 610$, $d/\eta = 5.9$, $\tilde{I} = 0.04$.

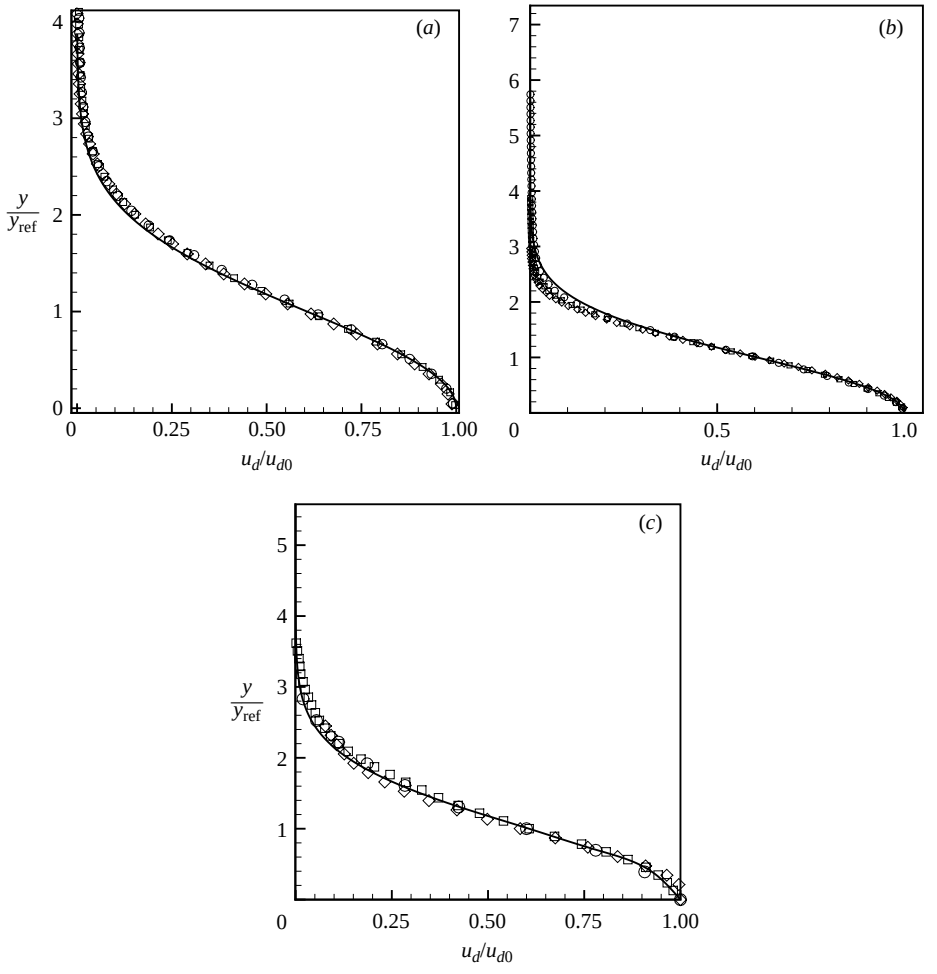


FIGURE 5. Mean velocity deficit in turbulent flows at different streamwise locations compared to the Gaussian profile. (*a*) Case 1 ($d/\eta = 1.53$, $I = 0.1$, $\langle Re_r \rangle = 107$), (*b*) case 3 ($d/\eta = 3.84$, $I = 0.1$, $\langle Re_r \rangle = 261$), (*c*) case 5 ($d/\eta = 9.59$, $I = 0.1$, $\langle Re_r \rangle = 610$). Solid line: Gaussian profile (3.1); ○, $x/a = 10$; □, $x/a = 15$; ◇, $x/a = 20$.

It was shown in the experiment of Wu & Faeth (1994*a*) that the particle wake in a turbulent flow behaves like a laminar wake and follows the simple law

$$\frac{u_d}{u_{d0}} = \exp[-(y/y_{\text{ref}})^2/2] \tag{3.1}$$

where $u_d$ is the mean velocity deficit, $u_{d0}$ is the mean velocity deficit at the wake centreline, and $y_{\text{ref}}$ is the cross-stream location where the mean velocity deficit becomes $e^{-1/2}$ times $u_{d0}$. In figure 5 we plot $u_d/u_{d0}$ obtained from the simulations for different $x$ locations along with the reference Gaussian profile given above. In agreement with the experimental results of Wu & Faeth (1994*a*), the present DNS results show that the turbulent wakes behave like self-preserving laminar wakes.

The centreline velocity deficit, $u_{d0}$, in a laminar wake decays as $1/x$. In figure 6 we plot the DNS result for the turbulent flow cases, and for the uniform flow case at $\langle Re_r \rangle = 610$, along with the theoretical prediction. The collapse of the data in the

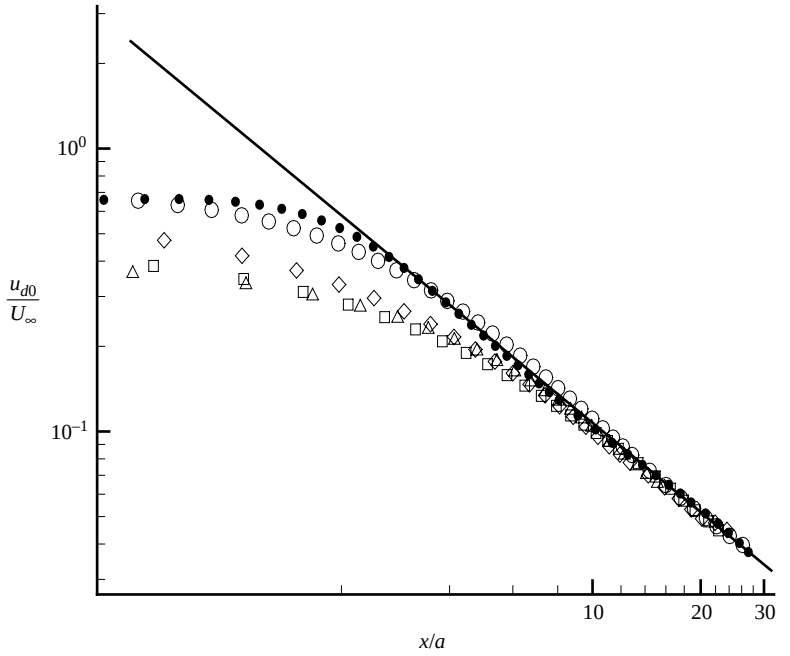


FIGURE 6. Mean velocity deficit along the wake centreline. Solid line represents $1/x$ decay of the self-preserving laminar wake. Symbols: ●, uniform flow at $\langle Re_r \rangle = 610$; ○, case 1 ($d/\eta = 1.53$, $I = 0.1$, $\langle Re_r \rangle = 107$); □, case 3 ($d/\eta = 3.84$, $I = 0.1$, $\langle Re_r \rangle = 261$); △, case 4 ($d/\eta = 3.84$, $I = 0.25$, $\langle Re_r \rangle = 114$), ◇, case 5 ($d/\eta = 9.59$, $I = 0.1$, $\langle Re_r \rangle = 610$).

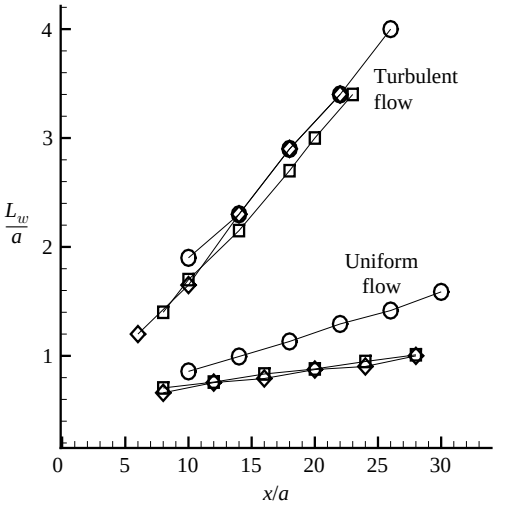


FIGURE 7. Half-width of the mean wake in uniform and turbulent flow. ○, case 1; □, case 3; ◇, case 5.

far-wake region further supports the laminar-like behaviour of the particle wake in turbulent flow. The half-width of the mean wake defined as $y_{\text{ref}} = L_w$ is shown in figure 7. In the case of turbulent flows, the wake is wider and expands more rapidly than in a uniform flow.

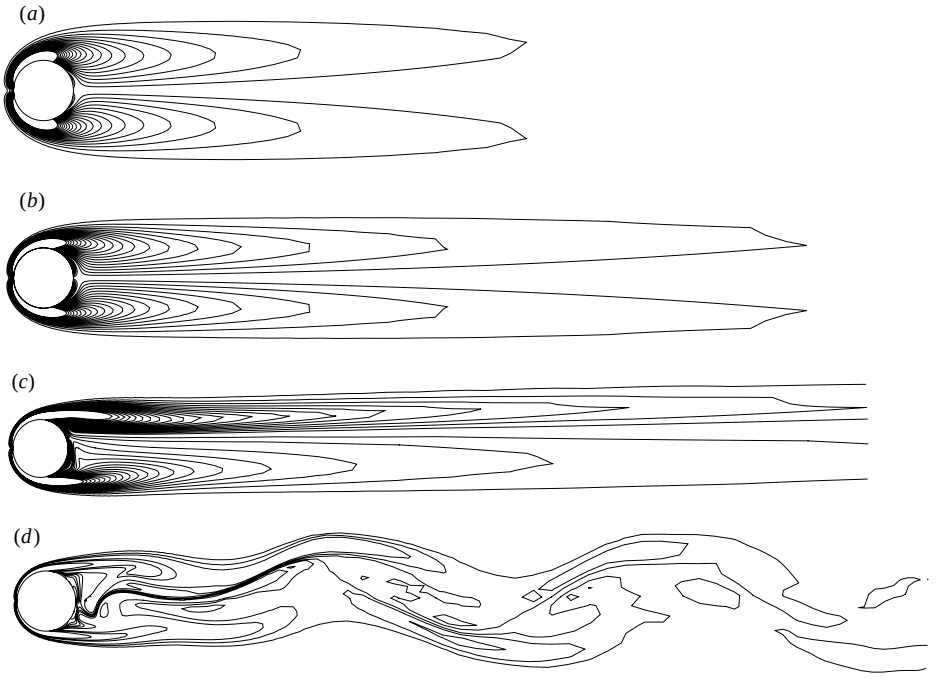


FIGURE 8. Azimuthal vorticity in uniform flow. (*a*) $\langle Re_r \rangle = 58$, (*b*) $\langle Re_r \rangle = 107$, (*c*) $\langle Re_r \rangle = 261$, and (*d*) $\langle Re_r \rangle = 610$. For (*d*) the flow is unsteady and hence contours at one time instant are shown.

### 3.2. *Time-dependent wake response*

In the range of particle Reynolds number considered here, the wake in a uniform flow exhibits three different structural regimes. For $\langle Re_r \rangle < 210$ the wake remains steady and axisymmetric, and the recirculation region appears as a toroidal vortex. At around $\langle Re_r \rangle = 210$, the first bifurcation occurs, and a non-axisymmetric wake appears in the form of two distinct thread-like vortical structures. The vortex structure remains symmetric about a plane passing through the centre of the particle. The double-threaded wake persists up to $\langle Re_r \rangle \approx 270$, beyond which unsteady vortex shedding appears. In this regime, three-dimensional structures in the form of vortex loops interconnected by streamwise elongated structures are generated. The planar symmetry is maintained in the wake even at a $\langle Re_r \rangle$ as high as 610. Figures 8 and 9 show the azimuthal vorticity on the ($x$, $y$)-plane, and the three-dimensional wake structure, respectively, for the uniform free stream. For the case of $\langle Re_r \rangle = 610$, results at one time instant are shown, since the flow is unsteady. The three-dimensional structure is extracted by an iso-surface of swirling strength, defined as the imaginary part of the complex-conjugate eigenvalue of the velocity gradient tensor (Zhou *et al.* 1999). In these computations the ($x$, $y$)-plane emerges as the plane of symmetry in both the $\langle Re_r \rangle = 261$ and 610 cases.

The time-dependent response of the wake to free-stream turbulence is shown in figures 10 to 12. Owing to free-stream turbulence, the wake is unsteady even at the lowest $\langle Re_r \rangle$ of 58 considered here. Figure 10 shows contours of azimuthal vorticity on a single plane containing the $x$-axis for the different cases at a particular instant in time. The iso-surface of swirling strength shown in figure 11 displays the three-dimensional structure of the wake for the different cases. For selected cases the

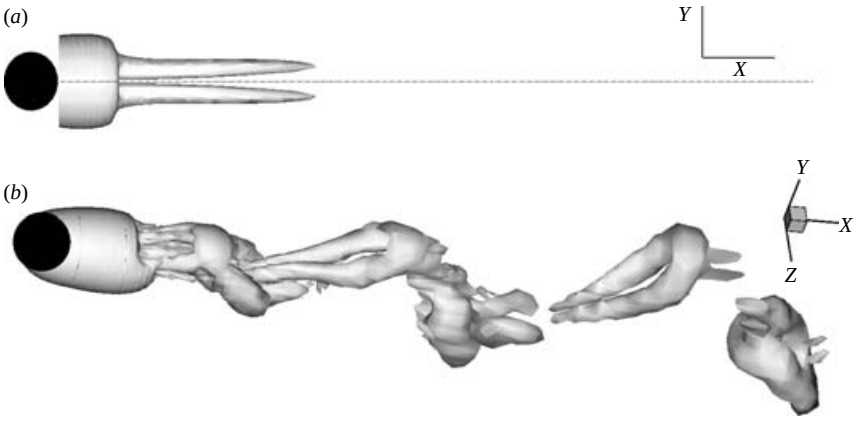


FIGURE 9. Three-dimensional vortex topology in uniform flow at (*a*) $\langle Re_r \rangle = 261$ and (*b*) $\langle Re_r \rangle = 610$. For (*b*) the flow is unsteady, and so one time instant is shown.

three-dimensional wake structure is displayed at two different time instants in order to illustrate its variability over time. In case 1 ($d/\eta = 1.53$, $I = 0.1$, $\langle Re_r \rangle = 107$), the toroidal vortex observed in a uniform flow is not greatly disturbed by free-stream turbulence. Occasionally a single or a double-threaded structure appears, which decays quickly as it advects downstream. The dominant effect of free-stream turbulence for this case is side-to-side time-dependent oscillation of the wake. For instance in figure 10(*a*) the wake can be observed to significantly tilt downward from the $x$-axis. The wake oscillation primarily arises out of the large-scale fluctuation in the free stream. The tilted wake in figure 10(*a*) can be considered as indicative of the downward tilting of the free stream at that instance. The oscillation of the wake in a turbulent flow is further illustrated in figure 12 where contours of zero streamwise velocity on the ($x$, $y$)-plane passing through the centre of the particle are shown at different times. Also shown are the zero streamwise velocity contours for the time-averaged velocity. The rear-end of the contour indicates the rear-most point of the recirculation region. The side-to-side movement of the wake is clear in figure 12(*a*). The length of the recirculation region and the separation point also vary in time. As can be expected the time-dependent wake significantly departs from axisymmetry. The behaviour of case 2 at $\langle Re_r \rangle = 58$ is similar to that of case 1 and is dominated by wake oscillation.

In case 3 ($d/\eta = 3.84$, $I = 0.1$, $\langle Re_r \rangle = 261$), the vorticity contours appear to be strongly influenced by free-stream turbulence. Wake oscillation is present, but more importantly, the shear layers now interact. As a result of this interaction isolated regions of vorticity detach from the sphere and are shed as wake vortices at regular interval. The steady double-threaded wake observed at a comparable Reynolds number in the uniform flow (see figure 9*a*) is significantly affected by free-stream turbulence. The two threads do not maintain their integrity, and they are now interconnected in a complex manner and elongated further downstream. Sometimes these regions of streamwise vortices are broken by free-stream turbulence and form $\Lambda$-shaped vortices. As will be seen below in velocity spectra, the shedding of vortices occurs at a preferred frequency. However, the structure of wake vortices induced by free-stream turbulence is somewhat different from those resulting from natural vortex shedding that occurs at supercritical Reynolds numbers. Nevertheless, the wake vortices in case 3 are observed to persist for a long distance downstream.

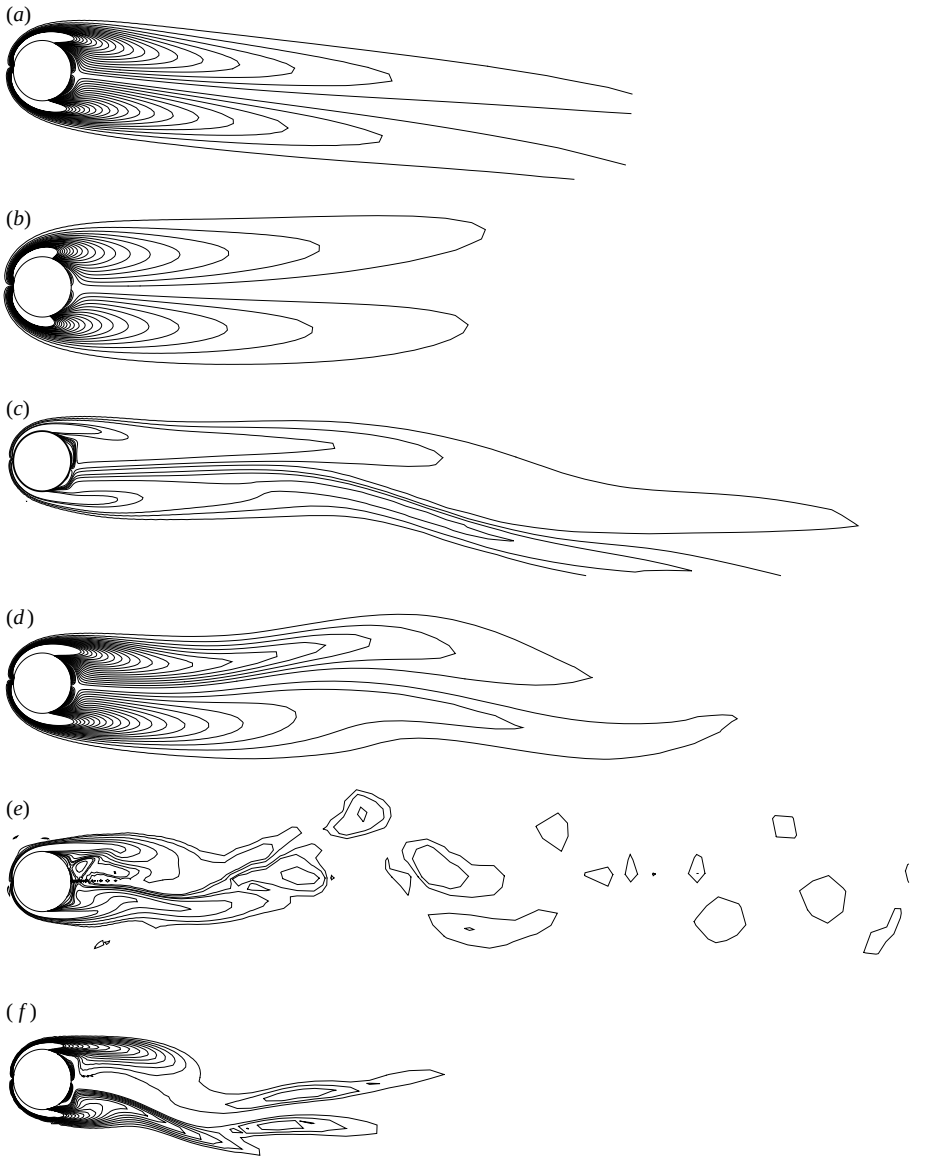


FIGURE 10. Azimuthal vorticity for turbulent flow cases. (*a*) Case 1 ($d/\eta = 1.53$, $I = 0.1$, $\langle Re_r \rangle = 107$), (*b*) case 2 ($d/\eta = 1.53$, $I = 0.2$, $\langle Re_r \rangle = 58$), (*c*) case 3 ($d/\eta = 3.84$, $I = 0.1$, $\langle Re_r \rangle = 261$), (*d*) case 4 ($d/\eta = 3.84$, $I = 0.25$, $\langle Re_r \rangle = 114$), (*e*) case 5 ($d/\eta = 9.59$, $I = 0.1$, $\langle Re_r \rangle = 610$), (*f*) case 6 ($d/\eta = 9.59$, $I = 0.25$, $\langle Re_r \rangle = 241$).

With further increase in turbulence intensity to $I = 0.25$ for the intermediate size particle (case 4), $\langle Re_r \rangle$ decreases to 114. As a result, the unsteadiness of the wake is dominated by wake oscillation and the behaviour is similar to that observed for cases 1 and 2. The streamwise elongated vortical regions disappear. However, the formation of large $\Lambda$-shaped vortices is still observed. Again note that the topology of these vortices is very different from that observed under natural vortex shedding in a uniform flow. Hence the subcritical vortex shedding process induced by free-stream turbulence is distinct from the natural vortex shedding process.

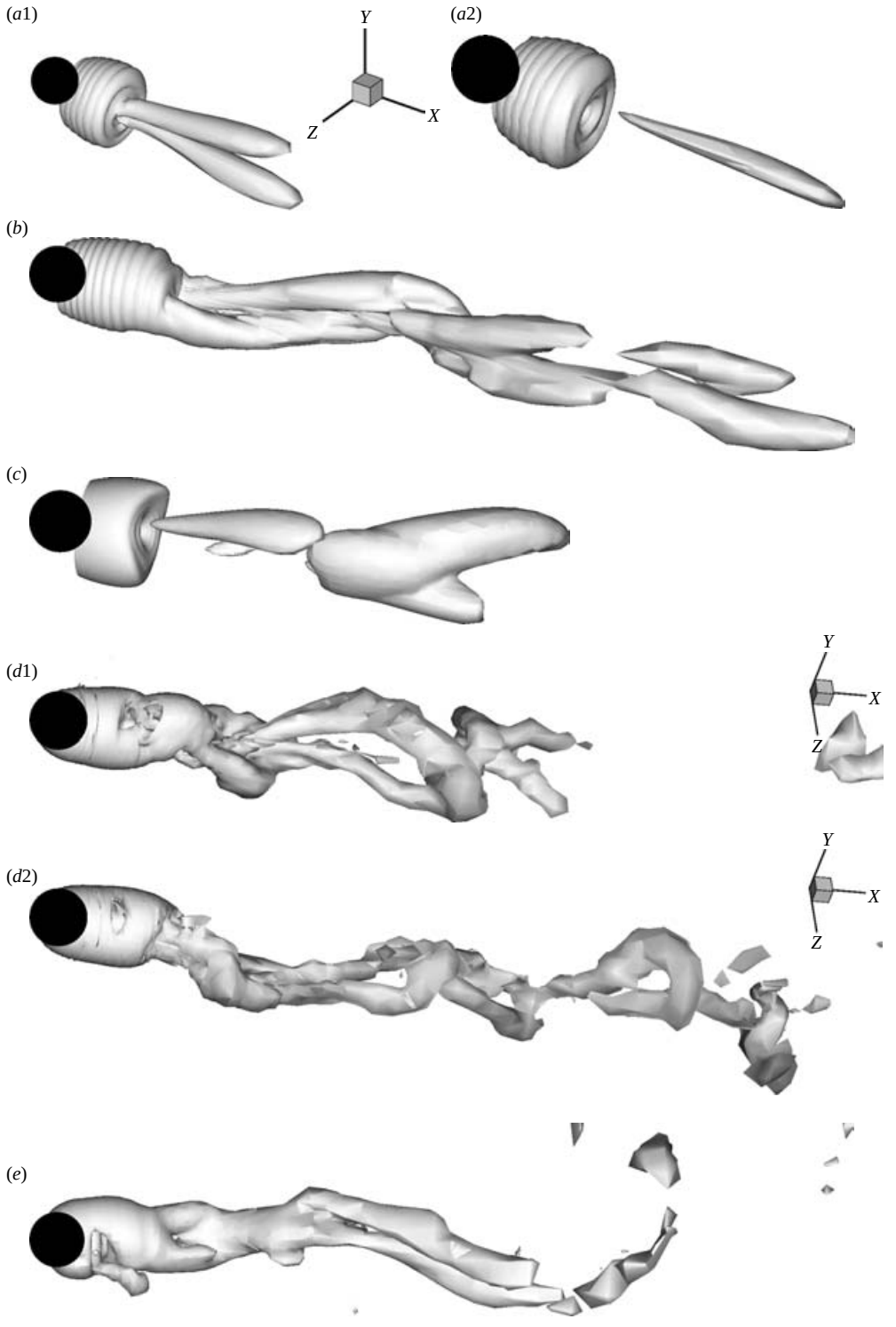


FIGURE 11. Three-dimensional vortex topology in turbulent flow. ($a1$, $a2$) case 1 ($d/\eta = 1.53$, $I = 0.1$, $\langle Re_r \rangle = 107$). ($b$) case 3 ($d/\eta = 3.84$, $I = 0.1$, $\langle Re_r \rangle = 261$). ($c$) case 4 ($d/\eta = 3.84$, $I = 0.25$, $\langle Re_r \rangle = 114$). ($d1$, $d2$) case 5 ($d/\eta = 9.59$, $I = 0.1$, $\langle Re_r \rangle = 610$). ($e$) case 6 ($d/\eta = 9.59$, $I = 0.25$, $\langle Re_r \rangle = 241$).

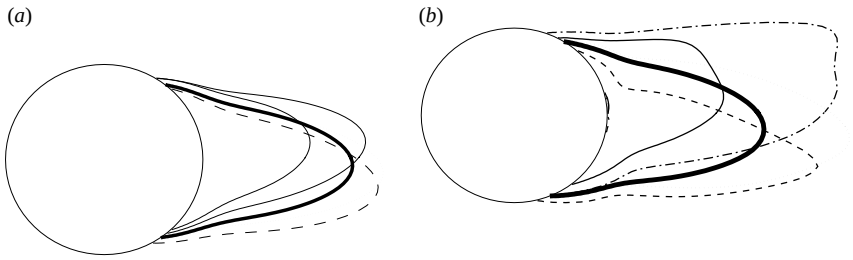


FIGURE 12. Wake oscillation shown by contours of zero streamwise velocity. The thick line is the contour obtained from the time-averaged velocity, and the thin lines are instantaneous contours at different times. (*a*) Case 1 ($d/\eta = 1.53$, $I = 0.1$, $\langle Re_r \rangle = 107$), (*b*) case 6 ($d/\eta = 9.59$, $I = 0.25$, $\langle Re_r \rangle = 241$).

For case 5 ($d/\eta = 9.59$, $I = 0.1$, $\langle Re_r \rangle = 610$) the vorticity contours indicate strong unsteady vortex shedding in the wake. However, in contrast to the uniform flow the shear layers are not stretched in the streamwise direction. Rather, they are shortened in length and broken into isolated patches of vorticity which quickly dissipate downstream. The three-dimensional wake structure exhibits unsteady vortex shedding similar to the case of uniform flow. However, the organized structures of interconnected vortex loops and streamwise vortices observed in the uniform flow (figure 9) are significantly distorted by free-stream turbulence. The vortex loops and streamwise connectors do not maintain their integrity any longer, and they are broken into smaller structures, which then quickly dissipate downstream. This is indicative of significantly enhanced fluctuations in the wake in the presence of free-stream turbulence.

In case 6 ($d/\eta = 9.59$, $I = 0.25$, $\langle Re_r \rangle = 241$), the shear layers indicate strong wake oscillation, and a weaker disorganized vortex shedding process. It is evident from figure 11(*e*) that at this higher free-stream turbulence intensity of $I = 0.25$, the vortex loops completely disappear, and the streamwise vortices are more reminiscent of the distorted double-threaded vortices seen earlier at the lower Reynolds numbers. In essence, free-stream turbulence is most influential in the intermediate range ($210 < \langle Re_r \rangle < 270$) when the wake becomes unsteady with shedding of $\Lambda$-vortices as opposed to a steady double-threaded wake. The above results on wake structure for the different cases are summarized in table 3. These results are in agreement with those of Mittal (2000). As discussed before, Mittal (2000) also observed that at intermediate $\langle Re_r \rangle$ the effect of turbulence is strong and $\Lambda$-shaped vortices are shed, while at higher $\langle Re_r \rangle$, natural vortex shedding is dominant.

### 3.3. *Spectra of near-wake and free-stream velocity traces*

Next we consider the spectra of the velocity traces in the near-wake region and in the free stream for all three particle sizes considered at $I = 0.1$ (figure 13). In the near-wake region, the velocity traces are first obtained at a point on the $x$-axis that is located at $2.5d$ from the centre of the particle. The free-stream velocity traces are obtained from the instantaneous relative velocity $\boldsymbol{V} + \boldsymbol{U}(\boldsymbol{X}_p(t))$ between the particle and the undisturbed ambient flow measured at the centre of the particle $\boldsymbol{X}_p(t)$. The spectra of the velocity traces are shown in figure 13 plotted with respect to the Strouhal number $St = fd/|\boldsymbol{V}_r|$ where $f$ is the frequency of oscillation. The spectra are obtained by Fourier transformation of the velocity traces collected over the time period $T$ taken by the box of isotropic turbulence to pass over the particle. For the smallest particle size (case 1: $d/\eta = 1.53$, $I = 0.1$, $\langle Re_r \rangle = 107$), the amplitude of oscillation of the

| Case | $d/\eta$ | $I$ | $\langle Re_r \rangle$ | Wake in uniform flow | Wake in turbulent flow |
|---|---|---|---|---|---|
| 1 | 1.53 | 0.1 | 107 | • Steady<br>• Axisymmetric | • Oscillating<br>• Nearly axisymmetric about instantaneous relative velocity<br>• Shear layers do not interact |
| 2 | 1.53 | 0.2 | 58 | • Steady<br>• Axisymmetric | • Oscillating<br>• Nearly axisymmetric about instantaneous relative velocity<br>• Shear layers do not interact<br>• Amplitude of oscillation nearly same as in case 1 |
| 3 | 3.84 | 0.1 | 261 | • Steady<br>• Non-axisymmetric<br>• Double-threaded wake<br>• Shear layers do not interact | • Unsteady vortex shedding $St = 0.12$<br>• $\Lambda$-shaped vortices<br>• Non-axisymmetric<br>• Complex wake topology<br>• Double-threaded wake is distorted and elongated further downstream<br>• Shear layers interact |
| 4 | 3.84 | 0.25 | 114 | • Steady<br>• Axisymmetric | • Unsteady vortex shedding<br>• $\Lambda$-shaped vortices<br>• Shedding is weaker than case 3<br>• No double-threaded wake |
| 5 | 9.59 | 0.1 | 610 | • Unsteady vortex shedding<br>• Coherent structure<br>• Streamwise elongated shear layers<br>• $St = 0.17$ | • Unsteady vortex shedding<br>• Irregular shapes<br>• Quickly dissipate downstream<br>• Shear layers are shortened and broken into smaller vortices<br>• $St = 0.17$ |
| 6 | 9.59 | 0.25 | 241 | • Steady<br>• Non-axisymmetric<br>• Double-threaded wake<br>• Shear layers do not interact | • Unsteady, strongly oscillating non-axisymmetric<br>• No distinct double-threaded structure<br>• Shear layers interact and break into smaller vortices |

TABLE 3. Summary of results on the effect of turbulence on the wake structure.

streamwise velocity in the near-wake region is increased for nearly all frequencies. The cross-stream spectrum, however, does not show any significant change and decays as in the free stream.

At the intermediate particle size of $d/\eta = 3.84$ (case 3), the amplitude of oscillation in the streamwise velocity increases at all frequencies, while that in the cross-stream velocity increases only at high frequencies above the shedding frequency. For larger particle at $d/\eta = 9.59$, a substantial increase in both the streamwise and cross-stream components can be observed.

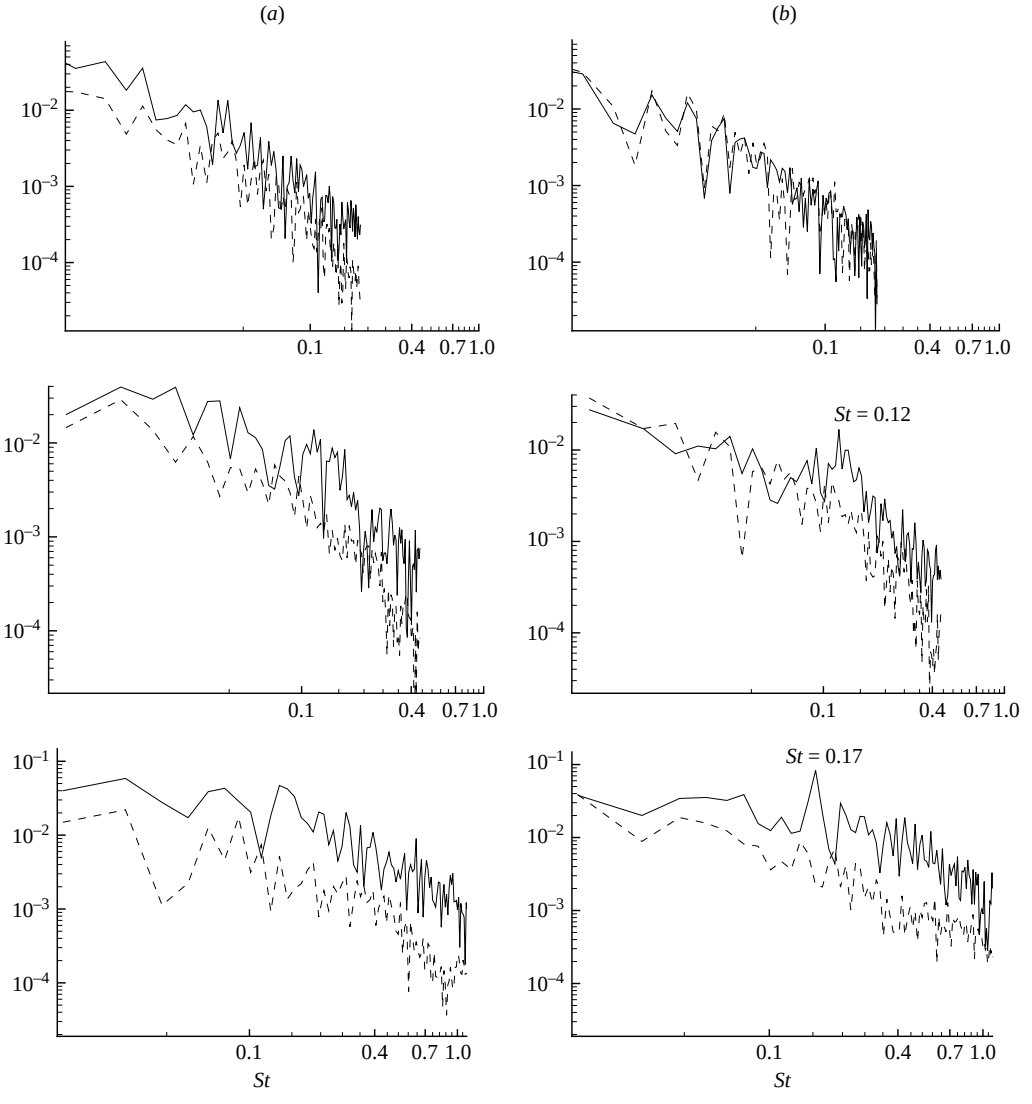


FIGURE 13. Spectra of the velocity traces for $I = 0.1$. ———, Near wake; - - - - - - -, free stream. (*a*) Streamwise velocity; (*b*) cross-stream velocity. Top: case 1 ($d/\eta = 1.53$, $I = 0.1$, $\langle Re_r \rangle = 107$), middle: case 3 ($d/\eta = 3.84$, $I = 0.1$, $\langle Re_r \rangle = 261$), bottom: case 5 ($d/\eta = 9.59$, $I = 0.1$, $\langle Re_r \rangle = 610$).

Similar results for the case of the higher turbulence intensity ($I = 0.2$ and 0.25) are shown in figure 14. The amplitude of free-stream oscillation has now increased due to higher values of $I$. But the velocity traces in the wake do not show any substantial increase compared with the previous case of $I = 0.1$. The spectra of both the cross-stream and streamwise velocities in the wake overlap with the corresponding spectra in the free stream.

For the small particle ($d/\eta = 1.53$) the spectra decay without any indication of characteristic frequency. As discussed above, the Reynolds numbers associated with the small particle (107 for $I = 0.1$ and 58 for $I = 0.2$) are sufficiently low that wake oscillation is the dominant mechanism. Wake oscillation is in response to free-stream

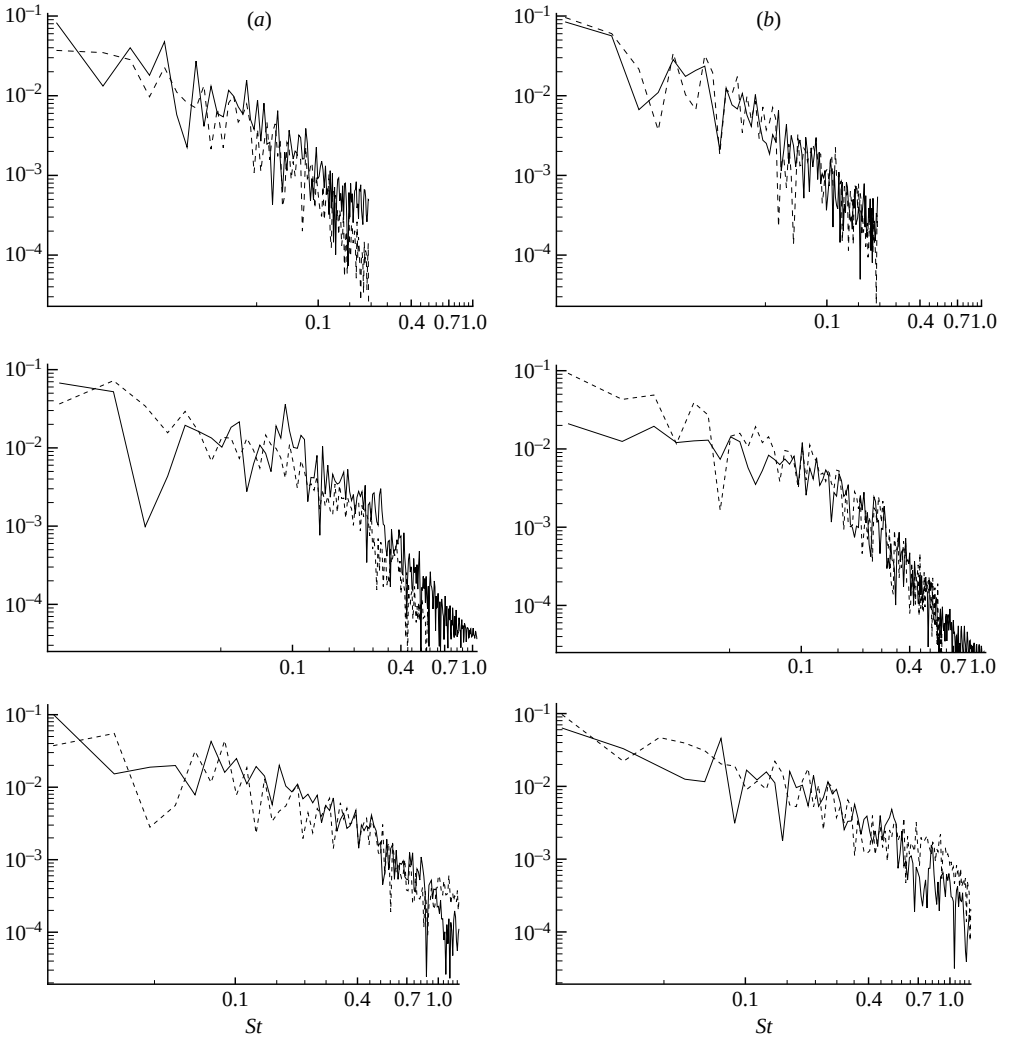


FIGURE 14. Spectra of the velocity traces for $I = 0.2$ and $I = 0.25$. ———, Near wake; - - - - - -, free stream. (*a*) Streamwise velocity; (*b*) cross-stream velocity. Top: case 2 ($d/\eta = 1.53$, $I = 0.2$, $\langle Re_r \rangle = 58$), middle: case 4 ($d/\eta = 3.84$, $I = 0.25$, $\langle Re_r \rangle = 114$), bottom: case 5 ($d/\eta = 9.59$, $I = 0.25$, $\langle Re_r \rangle = 241$).

turbulence and has no intrinsic frequency. The cross-stream velocity spectrum for the intermediate particle ($d/\eta = 3.84$, $I = 0.1$, $\langle Re_r \rangle = 261$) shows a local peak at around $St = 0.12$. There is no vortex shedding in a uniform flow at this $\langle Re_r \rangle$. However, if the shedding frequency observed at supercritical Reynolds numbers were to be extrapolated to $\langle Re_r \rangle = 261$, the corresponding Strouhal number can be estimated to be quite close to 0.12. Thus there is evidence to support early onset of vortex shedding in the presence of free-stream unsteadiness. This result is in agreement with the findings of Mittal (2000). At the higher free-stream turbulence intensity (case 4) there is modest peak in the streamwise velocity spectrum at $St = 0.1$, which could be associated with the $\Lambda$-vortices seen in figure 11(*c*), but a definitive signature of vortex shedding, usually present in cross-stream velocity spectra, is absent.

For the largest particle at $I = 0.1$ the cross-stream velocity shows a strong peak at $St = 0.17$ and somewhat weaker peaks at $St = 0.08$ and 0.03. A companion simulation for uniform flow past a sphere at $\langle Re_r \rangle = 610$ was performed to compare the results with turbulent and non-turbulent cases. The velocity trace and the spectra for the uniform flow at $\langle Re_r \rangle = 610$ show a dominant peak at $St = 0.19$ and two minor peaks at lower frequencies of $St = 0.08$ and 0.028. Thus, although wake vortex structures are altered by free-stream turbulence, the natural shedding mechanism appears to be still relevant at supercritical Reynolds numbers. At the higher free-stream turbulence intensity ($I = 0.25$) the Reynolds number decreases to 241 and is comparable to case 3. However, in contrast to case 3 shown in figure 13, the spectra for case 6 in figure 14 show no sign of a distinct vortex shedding frequency. This suggests that an early onset of vortex shedding is promoted only at modest levels of free-stream turbulence. Enhanced levels of free-stream turbulence can hinder the shedding process.

### 3.4. *Turbulence modulation in the wake*

First we will consider the distribution of the total kinetic energy in the vicinity of the particle. The objective here is to determine to what extent free-stream turbulence modifies the distribution of kinetic energy in the wake. The total kinetic energy is computed as

$$K_t = \tfrac{1}{2}\langle\langle \boldsymbol{u} \cdot \boldsymbol{u} \rangle\rangle, \tag{3.2}$$

where $\boldsymbol{u}$ defines the fluid velocity field and $\langle\langle\ \rangle\rangle$ indicates an average over time and along the azimuthal direction. The total kinetic energy is then scaled by the similarly defined total kinetic energy of the free stream, $K_t^0$

$$K_t^0 = \tfrac{1}{2}\langle\langle |\boldsymbol{V}_r^2| \rangle\rangle, \tag{3.3}$$

where $\boldsymbol{V}_r = \boldsymbol{V} + \boldsymbol{U}(\boldsymbol{X}_p(t))$ is the instantaneous relative velocity measured at the centre of the particle. Thus in this scaling the total kinetic energy of the fluid in the absence of the particle is unity. The distribution of total kinetic energy for case 1 is shown in figure 15. Also shown in the figure is the corresponding kinetic energy distribution for the uniform flow. The loss of energy in the near-wake region can be seen from the low values of the contours. The recovery of energy is more rapid in the case of turbulent inflow. The distribution for the other cases considered is qualitatively similar and therefore will not be presented here (see Bagchi 2002). The above result is clearly consistent with the reduction in wake length and the lower wake deficit observed earlier for the turbulent inflow.

The variation of the total kinetic energy along the $x$-axis in the particle wake is shown in figure 16. The results for the three different particle sizes are presented separately and the effect of increasing the free-stream turbulence intensity is presented. For comparison, the results for the corresponding uniform inflow are also shown (dashed lines), which we shall consider first. From the figure it is evident that recovery of total kinetic energy and approach to free-stream condition slows down with increasing $\langle Re_r \rangle$, provided the Reynolds number is less than about 280. The reduction is more pronounced as $\langle Re_r \rangle$ is increased from about 58 to 107, than from 114 to 261. With the onset of unsteady vortex shedding, however, the enhanced mixing in the wake significantly accelerates the approach to free stream.

For the small particle ($d/\eta = 1.53$), free-stream turbulence promotes more rapid recovery of the total kinetic energy. With increasing turbulence intensity from $I = 0.1$

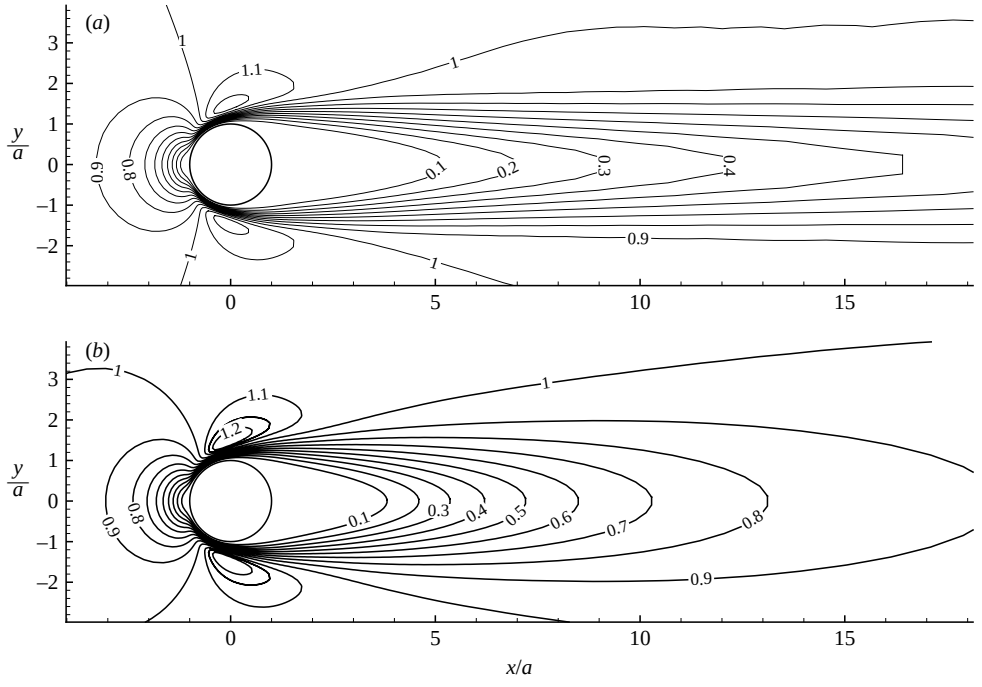


FIGURE 15. Contours of the total kinetic energy scaled by the free-stream total kinetic energy $K_t/K_t^0$ for case 1 ($d/\eta = 1.53$, $I = 0.1$, $\langle Re_r \rangle = 107$). (*a*) Uniform flow, (*b*) turbulent inflow.

to $I = 0.2$ the recovery is further accelerated. The rapid recovery is clearly due to enhanced mixing arising from the dominant wake oscillation. For the intermediate particle ($d/\eta = 3.84$) as well, free-stream turbulence significantly accelerates energy recovery in the wake. Interestingly, at the higher turbulence level of $I = 0.25$, the wake energy recovery is reduced, contrary to the behaviour for the smaller particle. This reduction is due to the fact that at the lower turbulent intensity ($I = 0.1$, $\langle Re_r \rangle = 261$) free-stream turbulence has induced vortex shedding, while at the lower $\langle Re_r \rangle$ corresponding to $I = 0.25$ the vortex shedding in the wake is still suppressed thereby reducing the level of mixing in the wake.

At $\langle Re_r \rangle = 610$ wake recovery is quite rapid, even for a uniform flow, due to the presence of natural vortex shedding. Thus, for case 5 ($d/\eta = 9.59$, $I = 0.1$, $\langle Re_r \rangle = 610$), the acceleration of energy recovery in the wake due to free-stream turbulence is not as significant as that observed for the smaller particles. As the turbulence intensity is increased to 0.25 (case 6), the recovery is faster in the near wake, but slower further downstream. This trend is because in case 6, the near-wake oscillation increases, but the shed vortices quickly dissipate downstream. However, compared with the uniform flow at $\langle Re_r \rangle = 241$, free-stream turbulence in case 6 contributes to a significant energy recovery in the wake.

The total kinetic energy can be divided into a contribution from the time-averaged mean flow and a contribution from fluctuations about the mean. The mean flow contribution pertains to the mean relative velocity between the particle and the free stream, and the resulting mean wake behind the particle. The kinetic energy contribution from fluctuations is of greater interest as it focuses on how the free-stream fluctuations are modulated in the particle wake. The kinetic energy due to

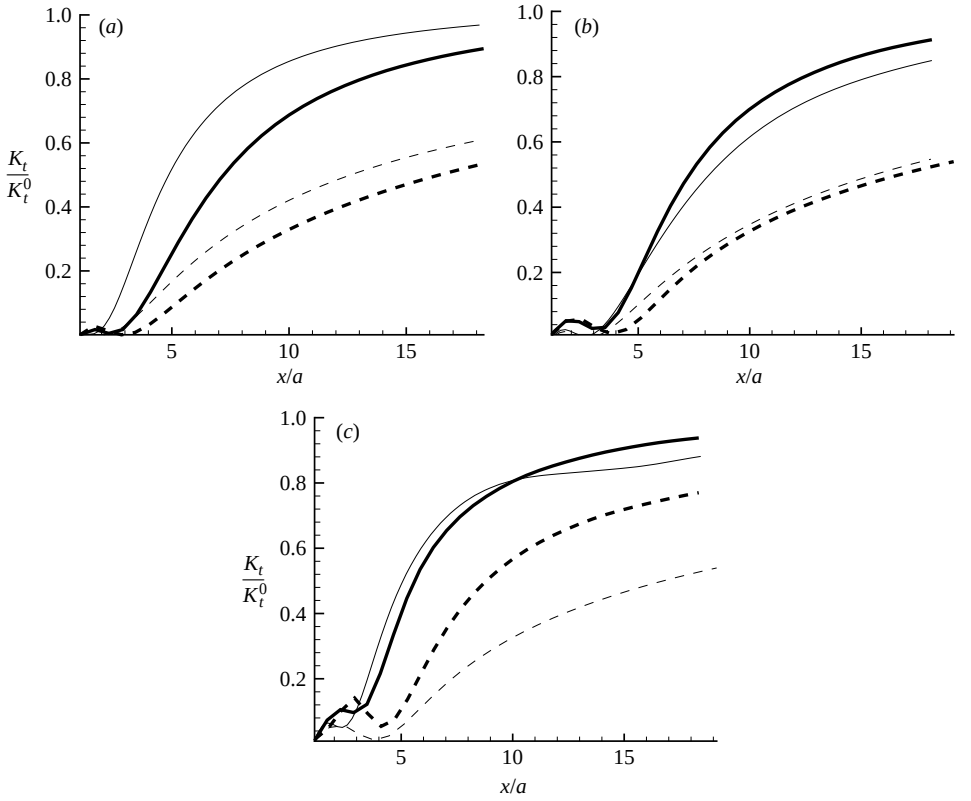


FIGURE 16. Total kinetic energy $K_t/K_t^0$ along the $x$-axis. (*a*) Cases 1 and 2 ($d/\eta = 1.53$), (*b*) cases 3 and 4 ($d/\eta = 3.84$), (*c*) cases 5 and 6 ($d/\eta = 9.59$). Thick lines are for $I = 0.1$, and thin lines for $I = 0.2$ or 0.25. Solid lines indicate turbulent flow, dashed lines indicate uniform flow.

fluctuations is defined as

$$K_f = \tfrac{1}{2}\langle\langle|\boldsymbol{u} - \langle\boldsymbol{u}\rangle|^2\rangle\rangle\,, \tag{3.4}$$

where $\boldsymbol{u} - \langle\boldsymbol{u}\rangle$ is the instantaneous velocity fluctuation about the time-average, $\langle\boldsymbol{u}\rangle$. Note that the above definition includes an average over the azimuthal direction as well. The fluctuating kinetic energy $K_f$ is normalized by the free-stream fluctuating kinetic energy $K_f^0$, defined as

$$K_f^0 = \tfrac{1}{2}\langle|\boldsymbol{U} - \langle\boldsymbol{U}\rangle|^2\rangle\,, \tag{3.5}$$

where $\boldsymbol{U} - \langle\boldsymbol{U}\rangle$ is the fluctuation in the ambient turbulence measured at the centre of the particle $\boldsymbol{X}_p(t)$.

In figure 17 the contours of $K_f/K_f^0$ are shown on a plane passing through the $x$-axis and by definition the distribution is symmetric about the wake centreline. The observed maximum value of $K_f/K_f^0$ is also presented in the figure and it indicates the degree to which the fluctuation energy is enhanced in the wake. Note that in all cases, far from the particle $K_f/K_f^0$ approaches the free-stream value of 1.0. For all three particle sizes, at the lower free-stream turbulent intensity of $I = 0.1$, fluctuating energy $K_f/K_f^0$ is enhanced in the wake. For the smallest particle considered (case 1; frame *a*), the increase in $K_f/K_f^0$ is primarily due to wake oscillation. At the intermediate size of

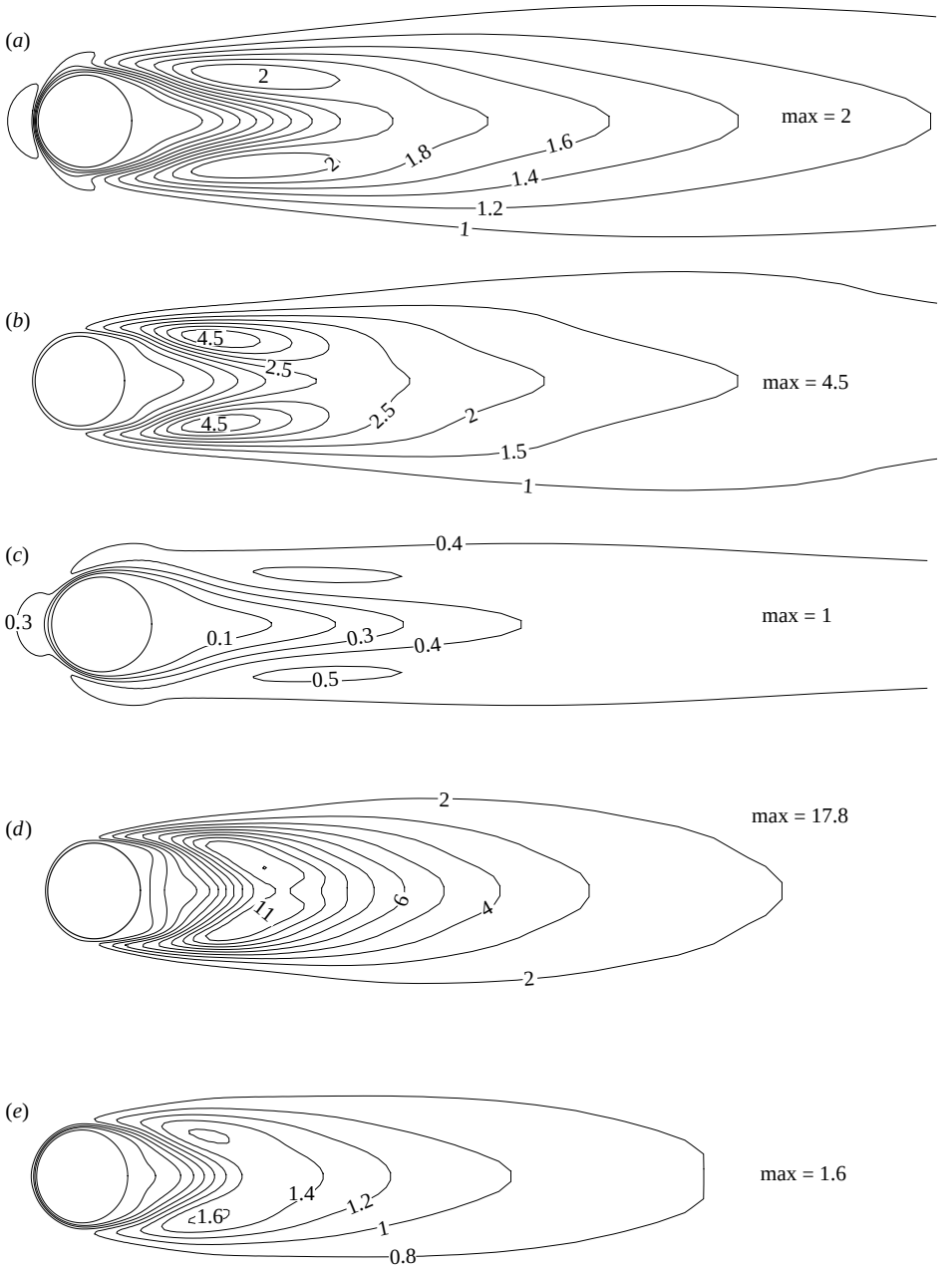


FIGURE 17. Distribution of the fluctuating turbulent kinetic energy normalized by the free-stream fluctuating kinetic energy, $K_f/K_f^0$. (*a*) Case 1 ($d/\eta = 1.53$, $I = 0.1$, $\langle Re_r \rangle = 107$), (*b*) case 3 ($d/\eta = 3.84$, $I = 0.1$, $\langle Re_r \rangle = 261$), (*c*) case 4 ($d/\eta = 3.84$, $I = 0.25$, $\langle Re_r \rangle = 114$), (*d*) case 5 ($d/\eta = 9.59$, $I = 0.1$, $\langle Re_r \rangle = 610$), (*e*) case 6 ($d/\eta = 9.59$, $I = 0.25$, $\langle Re_r \rangle = 241$).

$d/\eta = 3.84$ (case 3; frame *b*), the level of velocity fluctuation further increases, since the wake starts shedding vortices in addition to oscillating. For the larger particle of $d/\eta = 9.59$ (case 5; frame *d*), the local increase in fluctuating kinetic energy is as large as 18 times the free-stream energy. Such a substantial increase is due to the strong amplification of the vortex shedding process.

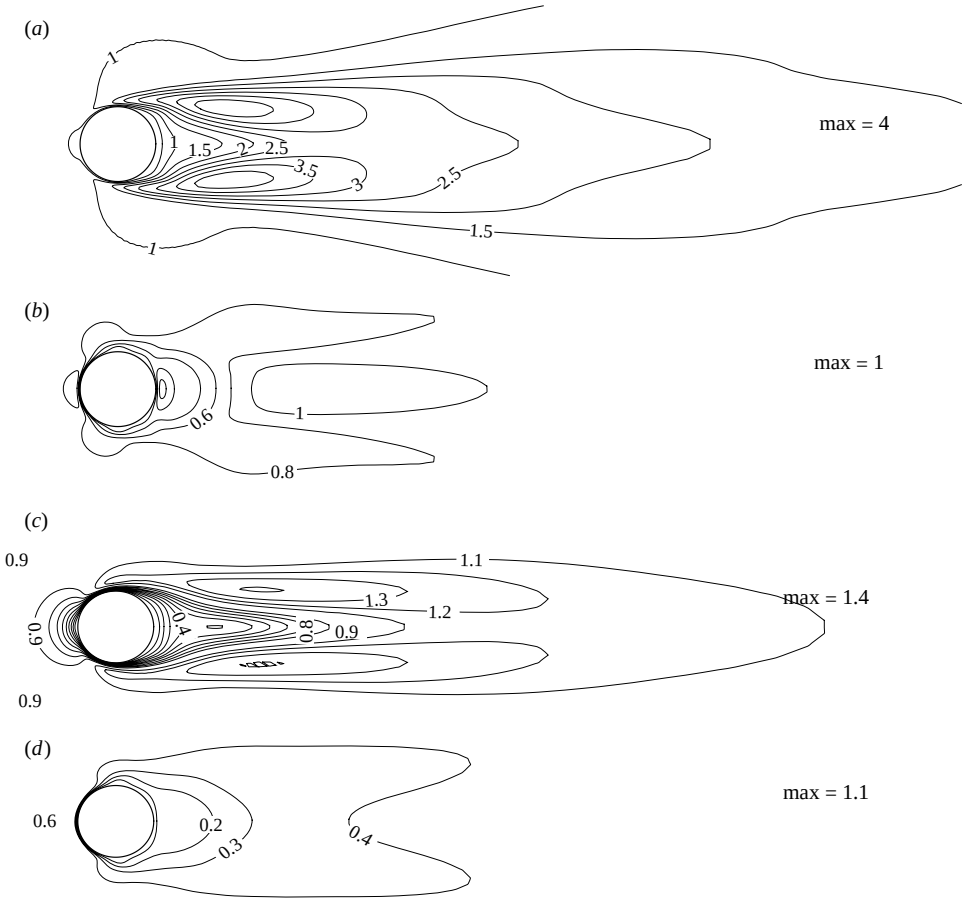


FIGURE 18. Contours of RMS velocity fluctuation scaled by the free-stream value for (*a*, *b*) case 3 ($d/\eta = 3.84$, $I = 0.1$, $\langle Re_r \rangle = 261$) and (*c*, *d*) case 4 ($d/\eta = 3.84$, $I = 0.25$, $\langle Re_r \rangle = 114$). (*a*) Streamwise component ($u'_x/U'_x$) for case 3, (*b*) cross-stream component ($u'_\rho/U'_\rho$) for case 3. (*c*) Streamwise component ($u'_x/U'_x$) for case 4, (*d*) cross-stream component ($u'_y/U'_y$) for case 4.

The case of the higher turbulence intensity is also shown in the figure. It is interesting to note that at the higher intensity of $I = 0.25$ the fluctuating energy $K_f/K_f^0$ is substantially damped over the entire wake for the intermediate size of $d/\eta = 3.84$ (case 4; frame *c*). The peak value of 1.0 is approached only away from the particle in the free stream. At $d/\eta = 9.59$ and $I = 0.25$ (case 6; frame *e*), $K_f$ is only marginally increased compared to $K_f^0$. This suggests that at low turbulent intensity, the level of velocity fluctuation in the wake is enhanced mostly by wake oscillation at low $\langle Re_r \rangle$ and by natural vortex shedding at high $\langle Re_r \rangle$. As the intensity of free-stream turbulence is increased, wake oscillation does not increase proportionately, and at higher $\langle Re_r \rangle$ the natural shedding can be disrupted. As a result, either a reduction or only a marginal increase in wake fluctuation energy is observed at the higher turbulent intensity.

Free-Stream turbulence at inflow is isotropic in nature; however, the mean relative velocity between the free stream and the particle introduces a preferred direction. Thus fluctuation in the neighbourhood of the particle will cease to be isotropic. We now address the statistical departure from isotropy by investigating the streamwise and cross-stream velocity fluctuations separately. These results for the intermediate and large particles are presented in figures 18 and 19, where the streamwise and

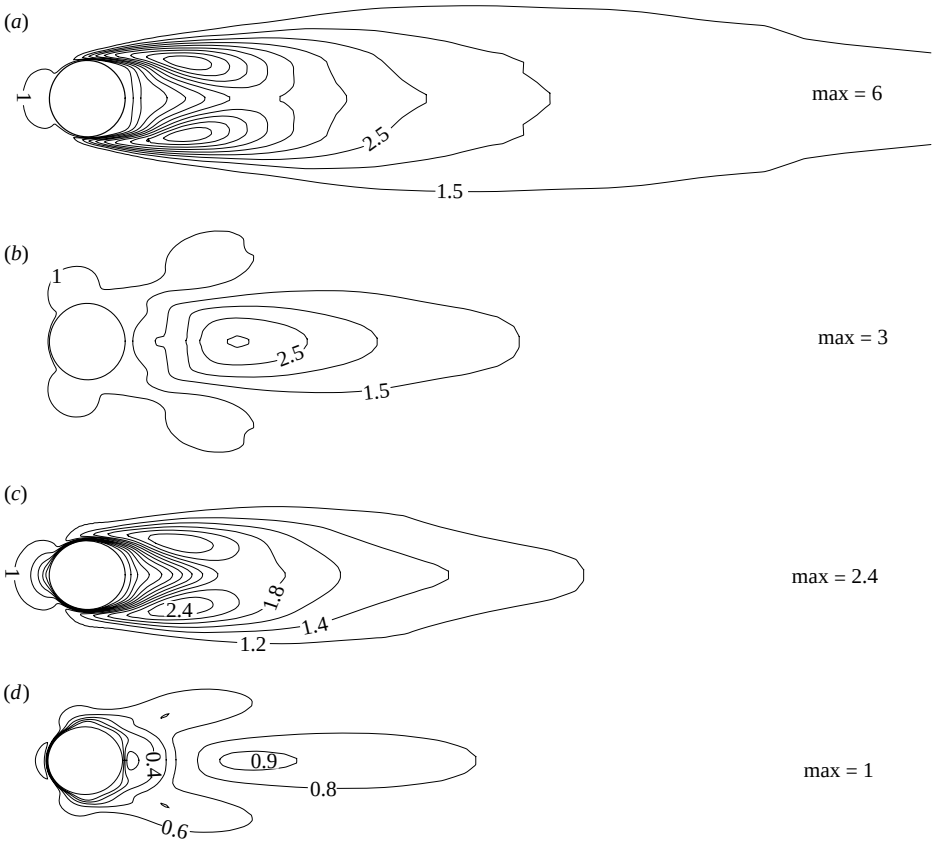


FIGURE 19. Same as figure 18 but for the larger particle (case 5: $d/\eta = 9.59$, $I = 0.1$, $\langle Re_r \rangle = 610$, (*a*) streamwise, (*b*) cross-stream) and (case 6: $d/\eta = 9.59$, $I = 0.25$, $\langle Re_r \rangle = 241$, (*c*) streamwise, (*d*) cross-stream).

cross-stream RMS fluctuations are scaled by the free-stream streamwise and cross-stream RMS fluctuations. The RMS streamwise and cross-stream velocity fluctuations, $u'_x$ and $u'_\rho$, are defined as

$$u'_x = \sqrt{\langle\langle (u_x - \langle u_x \rangle)^2 \rangle\rangle}, \quad u'_\rho = \sqrt{\langle\langle (u_\rho - \langle u_\rho \rangle)^2 \rangle\rangle}, \tag{3.6}$$

where $u_\rho$ is the radial velocity component in a cylindrical coordinate whose centre coincides with the centre of the particle, and the axial direction coincides with the streamwise direction $x$. Note that $\langle\langle\,\rangle\rangle$ denotes an average in time as well as over the azimuthal direction. Their free-stream counterparts, $U'_x$ and $U'_\rho$, are correspondingly given by

$$U'_x = \sqrt{\langle\langle (U_x - \langle U_x \rangle)^2 \rangle\rangle}, \quad U'_\rho = \sqrt{\langle\langle (U_\rho - \langle U_\rho \rangle)^2 \rangle\rangle}, \tag{3.7}$$

where $\boldsymbol{U}(\boldsymbol{X}_p(t))$ is the instantaneous ambient turbulent velocity measured at the centre of the particle. The normalized RMS fluctuations approach unity and hence statistical isotropy away from the particle. However, near the particle equi-partitioning of energy is clearly broken, mainly in the particle wake and to a lesser extent ahead of the particle. At the lower free-stream intensity, both the streamwise and cross-stream fluctuations are enhanced in the near wake. The increase in streamwise velocity

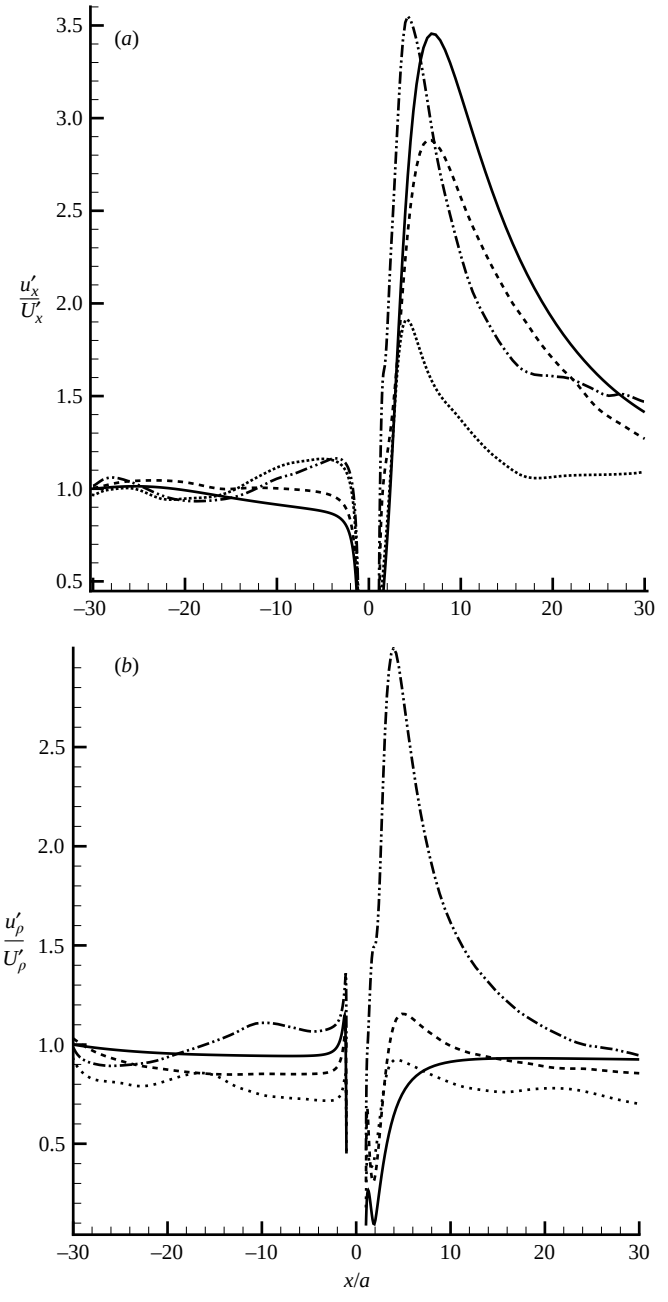


FIGURE 20. Root-mean square of (*a*) streamwise ($u'_x/U'_x$) and (*b*) cross-stream ($u'_\rho/U'_\rho$) fluctuations along the $x$ axis. ——, Case 1 ($d/\eta = 1.53$, $I = 0.1$, $\langle Re_r \rangle = 107$); - - - - - -, case 3 ($d/\eta = 3.84$, $I = 0.1$, $\langle Re_r \rangle = 261$); –··–··–, case 5 ($d/\eta = 9.59$, $I = 0.1$, $\langle Re_r \rangle = 610$); · · · · ·, case 6 ($d/\eta = 9.59$, $I = 0.25$, $\langle Re_r \rangle = 241$).

fluctuation is substantially more than that of cross-stream component. In fact, in case 3 at $\langle Re_r \rangle = 261$ the enhancement in cross-stream fluctuation is marginal and limited to only a small region in the wake; over the bulk of the wake cross-stream fluctuation is damped. The enhancement in streamwise and cross-stream fluctuations

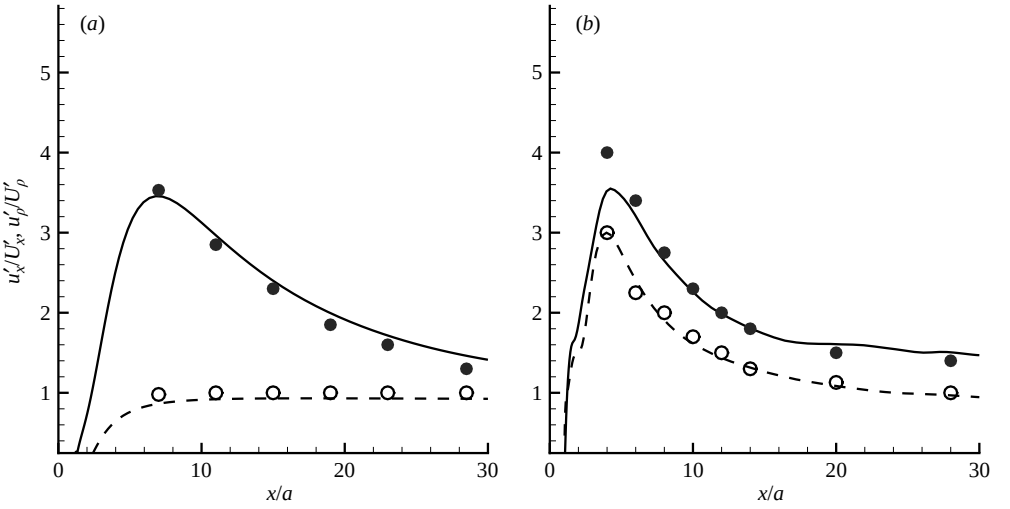


FIGURE 21. Comparison of the present DNS results with the experimental results of Wu & Faeth (1994*a*, *b*). Root-mean square of streamwise (solid lines and filled symbols) and cross-stream (broken lines and open symbols) fluctuations along the axis of the sphere normalized by the free-stream RMS are shown. Lines are the present results and symbols represent data read from Wu & Faeth. (*a*) Case 1 ($d/\eta = 1.53$, $I = 0.1$, $\langle Re_r \rangle = 107$) and (*b*) case 5 ($d/\eta = 9.59$, $I = 0.1$, $\langle Re_r \rangle = 610$). Note that the experimental data on cross-stream RMS for (*b*) are obtained from Wu & Feath (1994*b*). For all other cases, data are obtained from Wu & Faeth (1994*a*). The experimental data for case 1 correspond to $d/\eta = 1.25$, $\tilde{I} = 0.04$, $\langle Re_r \rangle = 135$, and for case 5 to $d/\eta = 5.9$, $\tilde{I} = 0.04$, $\langle Re_r \rangle = 610$.

is associated with early onset (in case 3) or reinforcement (in case 5) of natural vortex shedding by free-stream turbulence. When the free-stream turbulent intensity is increased to $I = 0.25$, for the largest particle (case 6), cross-stream fluctuations are again comparatively damped. The streamwise velocity fluctuations, although not damped, show a reduction in the level of enhancement. Similar behaviour is observed for the intermediate (case 4) as well as for the small particle (case 2; not shown here). The Reynolds numbers for cases 3 and 6 are comparable and a comparison of these two cases illustrates the role of free-stream intensity. Although case 6 corresponds to a larger particle, the corresponding RMS fluctuation is weaker, suggesting that vortex shedding (and in particular its early onset) is somewhat suppressed by the presence of very strong free-stream turbulence.

Figure 20 shows the normalized streamwise and cross-stream RMS fluctuations $u'_x/U'_x$ and $u'_\rho/U'_\rho$ along the $x$-axis. An extended region both upstream and downstream of the particle is shown. This figure provides some insight into the extent to which the presence of the particle influences the fluctuations downstream. First we note that the cross-stream RMS approaches the free-stream value faster than the streamwise RMS. In other words, the streamwise fluctuations persist for a longer distance downstream of the particle compared to the cross-stream fluctuations. As the free-stream intensity is increased to 0.25 (case 6, shown in the figure), both the streamwise and cross-stream RMS in the wake quickly approach the free-stream condition. It can be concluded that at low turbulence intensity anisotropy in the particle wake persists for a longer distance, whereas at higher intensity the wake is shortened and the isotropy of the free stream is quickly recovered.

In closing we discuss a comparison of the present DNS results on RMS fluctuations with the experimental results of Wu & Faeth (1994*a*, *b*) in figure 21. Normalized

fluctuations $u'_x/U'_x$ and $u'_\rho/U'_\rho$ are shown for case 1 ($d/\eta = 1.53$, $I = 0.1$, $\langle Re_r \rangle = 114$) and case 5 ($d/\eta = 9.59$, $I = 0.1$, $\langle Re_r \rangle = 610$). The experimental conditions of Wu & Faeth (1994*a*, *b*) are comparable to the present simulations; they considered a stationary particle subjected to homogeneous turbulence, although the microscale Reynolds number of the free-stream turbulence was different. Agreement between their experimental measurement and the results from the present DNS study is quite good. For the case of $d/\eta = 1.53$, both the streamwise and cross-stream RMS fluctuations are in good agreement. For the larger particle as well the cross-stream and streamwise fluctuations are in agreement, with the exception that the streamwise fluctuations in the experimental data are slightly higher near the particle, perhaps because the free-stream turbulence intensity in their experiment is about 4% and hence lower than the present case of about 10% intensity.

## 4. Summary and conclusions

The present direct numerical simulations considered the interaction of a single isolated stationary spherical particle with free-stream isotropic turbulence. The particle Reynolds numbers in the simulations range from about 50 to 600, the particle diameter is varied from about 1.5 to 10 times the Kolmogorov scale, and the free-stream turbulent intensity is 10% to 25% of the mean relative velocity. The pseudospectral methodology employed here resolves all the scales of free-stream turbulence and additional small scales generated in the shear layers and wake behind the particle. In order to assess the role of free-stream turbulence, for each of the turbulent cases considered a companion simulation was also performed, at the same mean Reynolds number, but in a uniform flow. The methodology and the results presented here are the first of their kind. A companion paper (Bagchi & Balachandar 2003) addressed in detail the effect of free-stream turbulence on the hydrodynamic force exerted on the particle. The purpose of this paper is to study the effect of free-stream turbulence on the particle wake and vortex shedding, and the modulation of free-stream turbulence in the particle wake. The computational setup and the parameters used in the present DNS are comparable to those employed by Wu & Faeth (1994*a*, *b*) in their experiments. It is shown that the DNS results are in good agreement with the corresponding experimental measurements. The major conclusions that can be drawn from this investigation are as follows.

(*a*) In a turbulent ambient flow the length of the mean (time-averaged) wake is reduced. The mean velocity profile shows that in the presence of free-stream turbulence the wake velocity deficit is reduced and the wake becomes flatter. The effect of free-stream turbulence is substantial at higher particle Reynolds numbers.

(*b*) In agreement with experimental observation (Wu & Faeth 1994*a*), the mean velocity profile in the particle wake in a turbulent free stream behaves like a self-preserving laminar wake.

(*c*) For mean particle Reynolds numbers below about 210, the effect of free-stream turbulence is to induce wake oscillation. Although vortical structures are occasionally shed, at such Reynolds numbers there is no regular vortex shedding. For Reynolds numbers below criticality (from 210 to about 280) free-stream turbulence promotes early onset of vortex shedding. The structure of wake vortices in the subcritical regime is somewhat different from that of natural shedding. At these intermediate Reynolds numbers the wake shows both oscillation and vortex shedding. For Reynolds numbers greater than 280, free-stream turbulence enhances the intensity of the unsteady vortex shedding process. However, unlike in a uniform flow, the vortices in the turbulent

flow do not maintain their integrity for a long time. Their evolution is more chaotic and they quickly dissipate downstream. At elevated levels of free-stream turbulence, there is evidence to suggest that free-stream turbulence, instead of aiding, can hinder and suppress the shedding process.

(*d*) A spectral analysis of the velocity traces in the wake suggests that for the case of low turbulence intensity, the amplitude of oscillation increases at all frequencies in the streamwise velocity component. The cross-stream component shows amplitude increase for frequencies above the shedding frequency. For the case of the higher turbulence intensity, no substantial increase in oscillation is observed.

(*e*) The effect of the particle on free-stream kinetic energy is studied in terms of both total and fluctuating energy. The total energy of the flow is significantly reduced in the wake due to wake deficit. In a turbulent ambient flow, the total energy in the wake is more rapidly recovered due to enhanced mixing.

(*f*) At low levels of free-stream turbulence, the fluctuating kinetic energy shows substantial enhancement in the wake, indicating local augmentation of turbulence. For the smallest particle considered, this enhancement is purely due to wake oscillation, whereas for the largest particle it is mostly due to vortex shedding. As the intensity of free-stream turbulence is increased, free-stream turbulence interferes with the wake vortex shedding process and as a result fluctuating kinetic energy in the wake is either damped or marginally increased.

(*g*) The fluctuating kinetic energy in the wake is not equi-partitioned among the streamwise and cross-stream components. The RMS streamwise fluctuation in the wake compared with that in the free-stream increases for all particle sizes and turbulence intensities considered here. On the other hand, the RMS cross-stream fluctuation increases only at the low turbulence intensity, and decreases at the higher turbulence intensity. The streamwise RMS, although not reduced, shows a reduction in enhancement with increasing free-stream intensity. Furthermore, at low levels of free-stream turbulence, statistical anisotropy in the particle wake persists for a longer distance downstream, whereas at higher free-stream intensity the statistical isotropy of the free-stream is quickly recovered.

The research is supported by the ASCI Center for Simulation of Advanced Rockets at the University of Illinois at Urbana-Champaign by the US Department of Energy grant (B341494). Computational facilities from the National Center for Supercomputing Applications, UIUC are greatly acknowledged.

## REFERENCES

Bagchi, P. 2002 Particle dynamics in inhomogeneous flows at moderate to high Reynolds numbers. PhD thesis, Department of Theoretical and Applied Mechanics, University of Illinois at Urbana-Champaign.

Bagchi, P. & Balachandar, S. 2002 Steady planar straining flow past a rigid sphere at moderate Reynolds number. *J. Fluid Mech.* **466**, 365–407.

Bagchi, P. & Balachandar, S. 2003 Effect of turbulence on the drag and lift of a particle. *Phys. Fluids* **15**, 3496–3513.

Boivin, M., Simonin, O. & Squires, K. D. 1998 Direct numerical simulation of turbulence modulation by particles in isotropic turbulence. *J. Fluid Mech.* **375**, 235–263.

Brucato, A., Grisafi, F. & Montante, G. 1998 Particle drag coefficients in turbulent fluids. *Chem. Engng Sci.* **53**, 3295.

Chen, J.-H. & Faeth, G. M. 2000 Continuous-phase properties of homogeneous particle-laden turbulent flows. *AIAA J.* **39**, 180–183.

Chen, J.-H., Wu, J.-S. & Faeth, G. M. 2000 Turbulence generation in homogeneous particle-laden flows. *AIAA J.* **38**, 636–642.

Clift, R., Grace, J. R. & Weber, M. E. 1978 *Bubbles, Drops and Particles.* Academic.

Elghobashi, S. E. & Truesdell, G. C. 1992 Direct simulation of particle dispersion in decaying isotropic turbulence. *J. Fluid Mech.* **242**, 655–671.

Gore, R. A. & Crowe, C. T. 1989 The effect of particle size on modulating turbulent intensity. *Intl J. Multiphase Flow* **15**, 279–285.

Hetsroni, G. 1989 Particle–turbulence interaction. *Intl J. Multiphase Flow* **15**, 735–746.

Johnson, T. A. & Patel, V. C. 1999 Flow past a sphere up to a Reynolds number of 300. *J. Fluid Mech.* **378**, 19–70.

Kulick, J. D., Fessler, J. R. & Eaton, J. K. 1994 Particle response and turbulence modification in fully developed channel flow. *J. Fluid Mech.* **277**, 109–134.

Langford, J. A. 2000 Toward ideal larger-eddy simulation. PhD Thesis, Department of Theoretical and Applied Mechanics, University of Illinois at Urbana-Champaign.

Longmire, E. K. & Eaton, J. K. 1992 Structure of a particle-laden round jet. *J. Fluid Mech.* **236**, 217–257.

Magarvey, R. H. & Bishop, R. L. 1961 Transition ranges for three-dimensional wakes. *Can. J. Phy.* **39**, 1418–1422.

Mittal, R. 2000 Response of the sphere wake to free-stream fluctuations. *Theore. Comput. Fluid Dyn.* **13**, 397–419.

Mittal, R. & Balachandar, S. 1996 Direct numerical simulation of flow past elliptic cylinders. *J. Comput. Phys.* **124**, 351–367.

Natarajan, R. & Acrivos, A. 1993 The instability of the steady flow past spheres and disks. *J. Fluid Mech.* **254**, 323–344.

Pan, Y. & Bannerjee, S. 1997 Numerical investigation of the effects of large particles on wall turbulence. *Phys. Fluids* **9**, 3786–3807.

Parthasarathy, R. N. & Faeth, G. M. 1990 Turbulence modulation in homogeneous dilute particle-laden flows. *J. Fluid Mech.* **220**, 485–514.

Squires, K. D. & Eaton, J. K. 1991 Measurements of particle dispersion from direct numerical simulations of isotropic turbulence. *J. Fluid Mech.* **226**, 1–35.

Tomboulides, A. G. & Orszag, S. A. 2000 Numerical investigation of transitional and weak turbulent flow past a sphere. *J. Fluid Mech.* **416**, 45–73.

Tsuju, Y., Morikawa, Y. & Shiomi, H. 1984 LDV measurement of an air-solid two-phase flow in a vertical pipe. *J. Fluid Mech.* **139**, 417–434.

Tsuji, Y., Morikawa, Y., Tanaka, T., Karimine, K. & Nishida, S. 1988 Measurement of an axisymmetric jet laden with coarse particles. *Intl J. of Multiphase Flow* **14**, 565–574.

Wang, L.-P. & Maxey, M. R. 1993 Settling velocity and concentration distribution of heavy particles in homogeneous isotropic turbulence. *J. Fluid Mech.* **256**, 27–68.

Wu, J.-S. & Faeth, G. M. 1994*a* Sphere wakes at moderate Reynolds numbers in a turbulent environment. *AIAA J.* **32**, 535–541.

Wu, J.-S. & Faeth, G. M. 1994*b* Effect of ambient turbulence intensity on sphere wakes at intermediate Reynolds numbers. *AIAA J.* **33**, 171–173.

Zhou, J., Adrian, R. J., Balachandar, S. & Kendall, T. M. 1999 Mechanism for generating coherent packets of hairpin vortices in near wall turbulence. *J. Fluid Mech.* **387**, 353–396.